PL-TR-96-2138

MODELING OF ATMOSPHERIC AND IONOSPHERIC DISTURBANCES FROM SHALLOW SEISMIC SOURCES

John B. Davies
Charles B. Archambeau

University of Colorado Physics Department
Theoretical and Applied Geophysics Group (TAGG)
Campus Box 583
Boulder, CO 80309-0583

May 1996

Scientific Report No. 1

Approved for public release; distribution unlimited

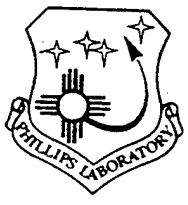

PHILLIPS LABORATORY
Directorate of Geophysics
AIR FORCE MATERIEL COMMAND
HANSCOM AFB, MA 01731-3010

"This technical report has been reviewed and is approved for publication."

DELAINE REITER
Contract Manager
Earth Sciences Division

JAMES F. LEWKOWICZ
Director
Earth Sciences Division

This report has been reviewed by the ESD Public Affairs Office (PA) and is releasable to the National Technical Information Service (NTIS).

Qualified requestors may obtain copies from the Defense Technical Information Center. All others should apply to the National Technical Information Service.

If your address has changed, or you wish to be removed from the mailing list, or if the addressee is no longer employed by your organization, please notify PL/IM, 29 Randolph Road, Hanscom AFB, MA 01731-3010. This will assist us in maintaining a current mailing list.

Do not return copies of this report unless contractual obligations or notices on a specific document requires that it be returned.

REPORT DOCUMENTATION PAGE

Form Approved
OMB No. 0704-0188

1. AGENCY USE ONLY (Leave blank)	2. REPORT DATE	3. REPORT TYPE AND DATES COVERED
	May, 1996	Scientific Report No. 1

4. TITLE AND SUBTITLE
Modeling of Atmospheric and Ionospheric Disturbances from Shallow Seismic Sources.

5. FUNDING NUMBERS
F19628-95-C-0197
PE 62601F
PR7600TAGM WU AF

6. AUTHOR(S)
John B. Davies and Charles B. Archambeau

7. PERFORMING ORGANIZATION NAME(S) AND ADDRESS(ES)
Theoretical and Applied Geophysics Group (TAGG)
University of Colorado Physics Department
Campus Box 583
Boulder, CO 80309-0583

8. PERFORMING ORGANIZATION REPORT NUMBER
153-5622

9. SPONSORING/MONITORING AGENCY NAME(S) AND ADDRESS(ES)
Phillips Laboratory
29 Randolph Road
Hanscom AFB, MA 01731-3010

Contracting Manager: Delaine Reiter

10. SPONSORING/MONITORING AGENCY REPORT NUMBER
PL-TR-96-2138

11. SUPPLEMENTARY NOTES

12a. DISTRIBUTION/AVAILABILITY STATEMENT
Approved for public release; distribution unlimited

12b. DISTRIBUTION CODE

13. ABSTRACT *(Maximum 200 words)*

Identification of seismic sources is enhanced by combining seismic detection methods with detection of the ionospheric disturbances caused by explosion and earthquake sources. In this study, numerical models of non-linear gravity controlled atmospheric disturbances produced by seismic sources near the surface of the earth are investigated in order to obtain quantitative predictions that can be used in evaluating detection methods based on gravity wave excitation. Explicit numerical integration of the non-linear finite difference equations is used to simulate the transient flows produced in a three-dimensional ARDC atmosphere. Results from the simulations agree with many results from linear theory approximations and also show non-linear characteristics similar to important gravity wave observations. Electron density changes in the ionosphere are predicted with their spatial and temporal behavior found to be particularly sensitive to the type and magnitude of the dissipative mechanisms that may occur. In the numerical examples studied, the amplitudes of the ionospheric electron density fluctuations due to the gravity waves produced by large explosions and some types of large earthquakes are predicted to be well within the range of detection using E-M ionospheric sounding methods.

14. SUBJECT TERMS
Ionospheric Seismic Earthquakes
Discrimination Explosions Nuclear

15. NUMBER OF PAGES
52

16. PRICE CODE

17. SECURITY CLASSIFICATION OF REPORT	18. SECURITY CLASSIFICATION OF THIS PAGE	19. SECURITY CLASSIFICATION OF ABSTRACT	20. LIMITATION OF ABSTRACT
UNCLASSIFIED	UNCLASSIFIED	UNCLASSIFIED	UNLIMITED

Table of Contents

INTRODUCTION

The primary objective of this study is to accurately predict the amplitudes and wave forms of low frequency gravity waves in the atmosphere and the ionosphere, which are produced by earthquakes and explosions. Since these waves, which increase in amplitude with altitude because of the decreasing density of the atmosphere with height, will produce relatively large fluctuations in the electron densities in the ionosphere, the disturbance can be sensed by standard electromagnetic sounding techniques. Hence, sensitive monitoring of seismically produced atmospheric disturbances can be accomplished by EM sounding methods. An objective of this study is, therefore, to produce predictions of the principal ionospheric disturbances to be expected from different kinds of shallow seismic sources, so that their characteristic atmospheric wave signatures can be used, along with seismic methods, to identify and characterize the sources. In addition, such predictive capabilities provide a framework for studying the properties of the atmosphere and ionosphere using gravity wave excitation produced by large seismic sources.

Near-surface sources can produce waves in the atmosphere having two principal components at long distances from the source, an acoustic wave with relatively high frequencies and a gravity wave with lower frequencies. Atmospheric and ionospheric disturbances due to seismic sources have been observed by numerous techniques and experiments. A review of the earlier observations is given by BLANC (1985), where earthquakes and volcanic eruptions were found to have produced atmospheric and ionospheric disturbances both near to, and very far from, their epicenters (DAVIES and BAKER 1965). In several early studies, nuclear explosions in the atmosphere were observed through their ionospheric effects (BENYON and JONES, 1962, BAKER and DAVIES, 1968, FRANCIS, 1975). There have also been recent observations of acoustic-gravity waves in the thermosphere following space shuttle ascents (JACOBSON and CARLOS, 1994).

Electromagnetic sounding of the ionosphere after surface explosions has concentrated on the initial acoustic response to the blast wave in the local region around the source (*e.g.*

BLANC and RICKEL, 1989). However, a surface chemical explosion of 5 kilotons (ANFO) was observed to excite 6 minute oscillations of the ionosphere that lasted for about 1 hour (JACOBSON, CARLOS and BLANC, 1988). KANAMORI et al., (1994), have evaluated observations for several major volcanic eruptions and have found 5-minute oscillations recorded near the Mt. St. Helens and Krakatoa volcanic eruptions with amplitudes of 0.3 mbar and 2 mbar respectively. Further, larger scale ionospheric motions, produced by long period gravity waves from earthquakes and subsurface nuclear explosions, are likely to be responsible for the observations of electromagnetic signals reported by GOKHBERG *et al.*, (1990).

The significance of the 5-minute oscillations is that this period closely corresponds to the theoretical Brunt-Vaisala period; that is, it is near to the theoretical minimum period for internal gravity wave oscillations in the atmosphere, for its particular density decrease with height. Extensive observations of the distribution of gravity waves, both in frequency and horizontal wave number space, indicate that the observed minimum period at the shorter wavelengths is, in fact, 5 minutes (MANSON, 1990). Likewise, the observed frequency distribution of gravity waves has been shown to be a consequence of both wave growth, due to decreasing atmospheric density with height, and wave dissipation (c.f. IMAMURA and OGAWA, 1995).

Since observations of zonal winds at 86 km altitude have shown that the background spectral density is a minimum at the Brunt-Vaisala frequency, with a spectral slope of about -5/3 for frequencies higher than those in the tidal band (FRITTS, 1984), it follows that the 5 to 10 minute period band is relatively noiseless and so gravity waves in this period range should be more readily observable. In this regard, recent observations and analysis of nightglow and noctilucent clouds at 80 to 130 km altitudes has allowed the direct observation of such waves (c.f. GARDNER, 1995, and associated papers). In addition, since gravity waves refract along the Earth's surface, they are observed at greater horizontal distances than the acoustic wave (FRANCIS, 1975). Thus, it is evident from the standpoint

of detectability that the 5 to 10 minute period gravity wave produced by a seismic source will be the most easily measured at high altitudes near the source.

As noted above, it has been demonstrated that wave growth, due to the decrease with altitude of the density of the atmosphere, occurs exponentially with a lower scale height of about 8 km, and it is also known that this growth is counteracted by damping due to radiation and molecular diffusion processes below the ionosphere, with the damping magnitude being dependent on the frequency and wavelengths of the internal gravity wave (IMAMURA and OGAWA, 1995). However, gravity waves near the Brunt-Vaisala frequency, and of shorter wavelength, are less affected by these damping processes and can grow to a saturation point where wave-breaking with viscous damping and other nonlinear processes can occur. Observations indicate that the saturation amplitudes of the internal gravity waves, occurring at about 80 km, are approximately 10% of the background fluctuations in the temperature and pressure fields at that altitude, with the gravity wave amplitude decreasing above this altitude (FRITTS, 1984). Further, the dissipative forces are found to be such that short-duration sources produce far-field gravity waves with wavetrains from 1 to 2 hours in duration. In the non-linear modeling developed in the present study, we will incorporate specific damping mechanisms and compare predicted results with observations in order to confirm that the modeling reproduces observations.

Based on partial confirmation of the non-linear numerical modeling by these limited observational results and verified, albeit approximate, analytical results, we will use predictions of amplitudes and wave characteristics in the time domain to evaluate the possibilities for observational studies using particular atmospheric and ionospheric gravity wave detection methods. In this regard, we compare correlations between the non-linear gravity wave predictions of this study and the GPS detections of ionospheric perturbations obtained by Calais and Minster (1995) following the large January 17, 1994 Northridge earthquake in order to try to establish a framework for further investigations.

CONSERVATION RELATIONS FOR ATMOSPHERIC MOTIONS

We use the primitive system where the continuity equations are based on the values of the continuum fields at particular points in space and time. Conservation of mass is expressed as :

$$\frac{\partial \rho}{\partial t} + \frac{\partial}{\partial x_j}(\rho v_j) = 0 \tag{1}$$

where ρ is density and v_j is velocity in the x_j direction. Conservation of momentum is expressed as :

$$\rho\left[\frac{\partial v_i}{\partial t} + v_j \cdot \frac{\partial v_i}{\partial x_j}\right] = \rho X_i + \frac{\partial}{\partial x_j} \cdot P_{ij} + F_i^{(d)} \tag{2}$$

where X_i are external forces such as gravity, and P_{ij} is the generalized stress, with:

$$P_{ij} = - p \cdot \delta_{ij} + 2\mu \cdot e_{ij} - 2/3\mu \cdot \delta_{ij} \cdot e_{kk} \tag{3}$$

Here, $e_{ij} = 1/2\left[\frac{\partial v_i}{\partial x_j} + \frac{\partial v_j}{\partial x_i}\right]$ is the strain rate and μ the viscosity. An effective force term $F_i^{(d)}$ is included to account for microscale momentum transfer that damps the mean velocity field v_i appearing in (2). This force will be referred to as a "drag force" and is usually taken to be proportional to velocity, with various phenomena such as turbulence and/or ion drag contributing in different altitude regions.

Conservation of energy gives the usual continuity equation governing temperature:

$$\rho \cdot \frac{\partial}{\partial t}(c_v \cdot T) + \rho v_j \cdot \frac{\partial}{\partial x_j}(c_v T) = \frac{\partial}{\partial x_j}(K \cdot \frac{\partial T}{\partial x_j}) - p \cdot \frac{\partial v_j}{\partial x_j} + \Phi^{(d)} + \Phi^{(v)} \tag{4}$$

where T is temperature, c_v is the specific heat at constant volume, K is the thermal conductivity and $\Phi^{(d)}$ the dissipation function involving drag and $\Phi^{(v)}$ the dissipation function involving viscous loss terms.

The equation of state for the atmospheric gas is taken to be ideal i.e.

$$P = \frac{k_B}{m} \cdot \rho \cdot T \tag{5}$$

where k_B is Boltzmann's Constant and m is the mean molecular weight.

In the fundamental equations, (1) through (5), the dependent and independent variables are now normalized with respect to typical values. For an ambient atmosphere with exponential decay of density with height, distances are normalized through the scale height, H, which, at the surface, is approximately 8400 metres. Velocities are normalized with respect to c_s, the sound velocity of air at the earth's surface. Thus, the Mach Number is just v/c_s where v is a typical velocity of the flow. Similarly density, pressure and temperature are normalized to ambient surface values, and the independent time variable, t, is normalized by (H/c_s). This produces a set of dimensionless ratios related to the Mach and other well-known dimensionless numbers.

Thus, for the continuity of mass we get, as before,

$$\frac{\partial \rho}{\partial t} = - \frac{\partial}{\partial x_j}(\rho v_j) \tag{6}$$

where the new variables are now normalized and given the same symbol as the original variables. Incorporating gravity as an external force, the momentum conservation equation, (2), becomes upon normalization :

$$\frac{\partial v_i}{\partial t} = - v_j \cdot \frac{\partial v_i}{\partial x_j} - G_s \cdot g(z) \cdot e_z - \frac{A_2}{\rho} \cdot \frac{\partial P}{\partial x_i} + \frac{A_4}{\rho} \cdot \Psi_i + \frac{A_1}{\rho} F_i^{(d)} \tag{7}$$

where $G_s = (g_s \cdot H/c_s^2)$ is a combination of Mach Number and Froude Number and the dimensionless number $A_2 = p_s/(\rho_s \cdot c_s^2)$ combines the Euler and Mach Numbers. $A_4 = \mu_s/\rho_s c_s$ measures the ratio of viscous to inertial forces and combines the usual Reynolds and Mach Numbers and Ψ_i is the normalized viscous force, given by the spatial gradient of the viscous terms in the generalised stress equation (3) and where μ is normalized to μ_s , the viscosity at the surface. In the atmosphere, μ is usually taken to be constant for the molecular viscosity. The parameter $A_1 = H/(\rho_s c_s^2)$ normalises the drag force whose particular dependence will be discussed later.

In the case of the conservation of energy, the normalized equation is

$$\frac{\partial T}{\partial t} = - v_j \cdot \frac{\partial T}{\partial x_j} + A_8 \cdot \frac{\partial^2 T}{\partial x_j^2} - A_6 \cdot \frac{\partial v_j}{\partial x_j} + A_5 \, \Phi^{(v)} + A_7 \, \Phi^{(d)} \qquad (8)$$

where

$$A_5 = \mu_s \cdot \frac{k_B}{m \cdot c_v} \cdot \frac{c_s}{(p_s \cdot H)} = A_6 \cdot \frac{A_4}{A_2}$$

$$A_6 = \frac{k_B}{m \cdot c_v}$$

$$A_7 = c_s/(c_v \rho_s H T_s)$$

$$A_8 = A_6 \cdot K \cdot \frac{T_s}{(p_s \cdot c_s \cdot H)}$$

Here the thermal conductivity K is, as usual, taken to be constant for the atmosphere. The equation of state, on normalization, is

$$p = \rho \cdot T/m(z) \qquad (9)$$

since the ideal equation of state at the surface is $p_s = \frac{k_B}{m_s} \cdot \rho_s \cdot T_s$ where m_s is the surface value of mean molecular weight and m(z) is the height-dependent normalized value.

Because an acoustic-gravity wave is a perturbation on the existing atmospheric structure, we shall decompose the thermodynamic variables into two components; the background stationary component and the perturbation. However, we do not assume that the perturbation is small in either temporal or spatial distribution as the gravity wave can grow with altitude. Thus, expressing the normalised density as $\rho = \rho_0 + \rho_1$, where 0 indicates the stationary state and 1 indicates the perturbation, we get for the conservation of mass :

$$\frac{\partial \rho_1}{\partial t} = - \frac{\partial}{\partial x_j} [(\rho_0 + \rho_1) v_j] \qquad (10)$$

Similarly, for the velocity equation (7), we get :

$$\frac{\partial v_i}{\partial t} = - v_j \cdot \frac{\partial v_i}{\partial x_j} - \frac{G_s \rho_1}{\rho_0 + \rho_1} \cdot g(z) \cdot e_z - \frac{A_2}{\rho_0 + \rho_1} \cdot \frac{\partial P_1}{\partial x_i} + \frac{A_4}{\rho_0 + \rho_1} \cdot \Psi_i + \frac{A_1}{\rho_0 + \rho_1} F_i^{(d)} \qquad (11)$$

where P_1 is the perturbed pressure component. The temperature equation (8) becomes :

$$\frac{\partial T_1}{\partial t} = - v_j \cdot \frac{\partial (T_0 + T_1)}{\partial x_j} + A_8 \cdot \frac{\partial^2}{\partial x_j^2}(T_0 + T_1) - A_6 \cdot \frac{\partial v_j}{\partial x_j} + A_5 \cdot \Phi^{(v)} + A_7 \cdot \Phi^{(d)} \qquad (12)$$

where T_1 is the perturbed temperature component. The equation of state (9) becomes :

$$P_1 = (\rho_0 T_1 + \rho_1 T_0 + \rho_1 T_1)/m(z) \qquad (13)$$

The introduction of internal sources and sinks of energy and momentum is intended to account for processes which are poorly understood theoretically and are represented by parameterization (VOLLAND, 1988). In the atmosphere below the thermopause, the only dissipative mechanisms are molecular viscosity, thermal conductivity and interaction with the innate turbulence. The kinematic viscosity increases like the density decreases with height in the atmosphere. However, neither it nor the molecular thermal conductivity immediately affect the momentum and energy of these gravity waves below the thermosphere, as it takes a time of the order of days to damp these large wavelength systems (PITTEWAY and HINES, 1963). Thus, we ignore the molecular viscosity term Ψ_i in equation (11) and the $\Phi^{(v)}$ term in equation (12). Above the thermopause, it is expected that dissipation due to ion drag becomes important (MIESEN *et al.*, 1989).

Turbulence, at altitudes below the thermopause, is considered to be the most important drag force (DEARDORFF, 1985). In order to account more accurately for the inherent sub-grid scale turbulence in the atmosphere below the thermopause, the flow variables at a point can be decomposed into a mean flow and a perturbed turbulent flow (DEARDORFF, 1985). In the momentum continuity equation, additional components are thus obtained for the generalized stress, which are mainly interaction terms between the mean and perturbed densities and velocities, termed the Reynold's stresses, which represent the interaction of the mean flow with the sub-grid scale turbulence. These additional stresses have been approximated in various phenomenological approaches, including the introduction by Boussinesq of the concept of eddy

viscosities in order to use the Newtonian equations with the usual, but much larger, viscosity term. However, this equivalent viscosity approach has been shown to be unable to effectively model dissipation due to turbulence, and so other methods using Rayleigh friction have been invoked (VOLLAND, 1988).

We will, therefore, model the effects of turbulence on the gravity wave momentum through use of drag forces that are proportional to velocity. We incorporate these diverse sources of drag and dissipation into the force term $F_j^{(d)}$ that acts to reduce the mean velocity. That is, in eq: (7) we use:

$$F_j^{(d)} = -k^{(d)} \cdot v_j \tag{14}$$

where $k^{(d)}$ is a spatially dependent drag coefficient. Different drag components, due to differing mechanisms, will be operable at various altitudes and under various wind and ion conditions, so that $k^{(d)}$ can be explicitly altitude dependent. The effect of the dissipative mechanisms on the temperature equations are neglected, as we invoke the argument that energy loss from the large-scale gravity waves through interactions with large-scale turbulent motions takes a time of the order of days to decay into molecular size eddies and thereby input thermal energy into the system (PITTEWAY and HINES, 1963). Thus, the $\Phi^{(d)}$ term in eq: (12) will be neglected compared to other terms, since short term predictions are of interest.

The boundary conditions that apply express conservation of mass and momentum across surfaces of material discontinuity. They are simply expressed as the continuity of the normal component of particle velocity, for conservation of mass, and the continuity of tractions, for the conservation of momentum. That is:

$$\begin{aligned} \left\| v_j n_j \right\| &= o \quad \text{for } \mathbf{r} \in S \\ \left\| P_{ij} n_j \right\| &= o \quad \text{for } \mathbf{r} \in S \end{aligned} \tag{15}$$

where **r** denotes the position vector, **n** is the normal to the surface S, and the double bracket notation in (15) is used to represent the difference in the bracketed quantity across the surface S.

A seismic source, producing waves in the solid medium below the planetary atmosphere-lithosphere boundary (S_0), produces atmospheric excitation through the continuity equations in (15). From these conditions we see that the vertical component of the solid medium particle velocity is imparted to the atmospheric medium, while the other coupling is that of the atmospheric pressure to the solid medium traction on S_0. To first order the pressure changes in the atmosphere due to the traction variations produced by seismic waves are neglected and the boundary is treated as traction free. In this case, only the velocity condition in (15) produces time dependent momentum changes at the lower boundary of the atmosphere.

Thus, the atmospheric coupling due to a seismic source in the earth is quite predictable when the seismic wave field in the solid can be specified either numerically or analytically. Representations of wave fields from seismic sources of various kinds (e.g. earthquakes, chemical and nuclear explosions) can be made with accuracy, so that predictions of atmospheric excitation using the velocity boundary condition in (15) is quire straightforward. Here, the direct wave field from the seismic source plays the role of a forcing function on the atmosphere along the boundary at S_0, and will give rise to low frequency, long wavelength, atmospheric motions, including net flow components, as well as high frequency acoustic waves. In the case of earthquakes, and underground nuclear tests, which release most of their energy at depths well below S_0, the excitation of high frequency acoustic waves can be expected to be negligible compared to transport effects and the boundary movement excitation of the much lower frequency gravity waves.

The atmospheric motions are also the cause of ionospheric charged particle motions which can be approximated as following the motions of the neutral gas (KELLEY and

HYSELL, 1991). The basic conservation law for charged particles, assuming no creation or destruction, is:

$$\frac{\partial N_\alpha}{\partial t} = -\frac{\partial (N_\alpha \cdot v_j^\alpha)}{\partial x_j} \tag{16}$$

where N_α is the number of particles of type α and v_j^α is their velocity in the j'th direction. The particles of interest here are electrons, and the initial concentration of this charged particle is taken to be time-independent with only a vertical functional dependence, N(z). Since we are concerned with one particle type the subscript α will be dropped in the following. Assuming only small changes in this concentration, the time dependence can be found from integrating equation (16) over time. In this approximation the concentration change becomes:

$$\delta N(z,t) = -\frac{\partial N(z)}{\partial z} \cdot \int_{t_o}^{t} v_z(t')\, dt' - N(z) \cdot \int_{t_o}^{t} \frac{\partial v_j(t')}{\partial x_j}\, dt' \tag{17}$$

The first term in (17) is the concentration change due to the displacement of the ionospheric layer, while the second term arises as a result of compression or rarefaction and is the dominant term when dealing with processes involving characteristic dimensions smaller than the width of the layer. The velocity of the charged particles is usually taken to be of the order of that of the neutral gas and this approximation will be used in the calculations for electron density charges.

Therefore the neutral gas velocity, which is computed using equ: (10) - (13) is used in eq: (17) to predict the electron density changes in the ionosphere. In this latter computation, the initial concentration of electrons is taken to be that of a Chapman distribution. This distribution has a maximum density at 345 km height and decreases rapidly below about 90 km ,with the functional dependence on height defined by:

$$N(z) = N_c \cdot \exp\left[\frac{1}{2}\left(1 - \xi - e^{-\xi}\right)\right] \tag{18}$$

where $\xi = (z-h_c)/H$, h_c is 345 km, H is 65 km and N_c is a normalizing value equal to N at the altitude h_c.

Linear Approximations for Gravity and Internal Waves

Predictions of important features of the low frequency gravity and internal waves generated by surface atmospheric sources have been made using linearized approximations to the eq: in (10) through (13). Many of these predictions have been observationally verified, at least in the approximate sense of the theory itself. Therefore, the verified analytical results from linear approximations are important for physical insights and as criteria in evaluating results from non-linear numerical computations.

Although the full set of flow equations do not have analytical solutions, it has been shown that even weak non-linear analyses can yield solitary waves (MIESEN, 1992) and complex interactions (KLOSTERMYER, 1978). Linearization of the fundamental conservation equations is usually performed by removing terms that are of second order in particular physical situations. This approximation reduces the equ: (10) - (13) to:

$$\frac{\partial \rho_1}{\partial t} = -\frac{\partial}{\partial x_j}\left[p_o v_j\right] \tag{19}$$

$$\rho_o \frac{\partial v_i}{\partial t} = \rho_1 g(z)\cdot \mathbf{e}_z - \cdot\frac{\partial P_1}{\partial x_i} + \Psi_i + F_i^{(d)} \tag{20}$$

which apply only for flows and waves with quite low particle velocities and velocity gradients.

Internal gravity waves in density-stratified fluids are completely different from the familiar acoustic waves, as they are anisotropic and dispersive. After linearization, they are governed by hyperbolic differential equations, rather than the elliptical equations obtained in the linearized acoustic case. Thus, the gravity waves are anisotropic and dispersive and do not obey Fermat's principle (BARCILON and BLEISTEIN, 1969). Fourier decomposition of the linearized perturbation equations, with phase and group velocities assuming paramount importance, has been successful in analyzing these internal waves (LIGHTHILL, 1978). Here, the emphasis has been on initial perturbation problems and oscillating, or uniformly moving, sources. In the simplest case, the fluid is assumed unbounded, dissipative forces are ignored, the buoyancy (Brunt-Vaisala) frequency is assumed constant and the internal waves

are three-dimensional. Further, the Boussinesq approximation is assumed and this implies the neglect of the inertial effects of density variations compared with the buoyancy forces they create. Lighthill (1978) also argued, however, that when non-Bousinesq effects are taken into account, compressibility is important and the internal waves become acoustic-gravity waves.

In a stratified fluid, where the undisturbed density ρ_0 varies exponentially with height z according to

$$\rho_0(z) = \rho_{00} e^{-\beta z}$$

the buoyancy frequency N is given, in the linear approximation, by

$$N = (g\beta)^{1/2}$$

For the simplest case, the dispersion relation for plane monochromatic, Boussineq type internal waves (LIGHTHILL, 1978) is given by

$$\omega = N k_h / k$$

where k is the modulus of the wavevector and k_h is the modulus of its horizontal projection. This implies waves with a frequency $\omega<N$, for an arbitrary wavelength λ ,and an inclination of the planes of constant phase to the vertical of $\theta =$ arccos (ω / N). The phase velocity with which these planes move is perpendicular to the group velocity and, consequently, the fluid particles move along straight-line paths parallel to the wavecrests. In the non-Boussinesq case, the dispersion relation becomes (VOISIN, 1991):

$$\omega = N k_h / (k^2 + 0.25\beta^2)^{1/2}$$

Thus, the wavenumber surface is no longer a cone but a hyperboloid surface of revolution. The group velocity points along this surface normal, but it is no longer perpendicular to the wavevector, and the trajectories of fluid particles now become ellipses. A point monochromatic source thus radiates non-Boussinesq internal waves into the total region where $|\cos\theta| < \omega / N$, with a group velocity that is a maximum at a particular angle in this cone.

The more recent linear approach by VOISIN (1991) is based on a Green's function method, where the internal wave field is studied using a number of different Green's functions applicable under various specific conditions. Voisin shows that, in accordance with the group velocity approach used by Lighthill, internal waves propagate for frequencies in the range $N|\cos\theta| < |\omega| < N$, while outside this band they are evanescent with an exponential decay with distance from the source. Further, Voisin determines that impulsive internal waves are made up of the combination of gravity waves and buoyancy oscillations of the fluid; with the latter described by DICKINSON (1969).

In order to understand the separation of internal waves into gravity waves and buoyancy oscillations, asymptotic approaches are used. For a point source, at small times, the Boussinesq fluid motion essentially ignores its internal stratification and its motion is irrotational (BATCHELOR, 1967). At large times such that $Nt >> 1$, gravity waves and buoyancy oscillations become separated, with gravity waves having the phase expected from group velocity analysis while buoyancy oscillations are present but do not propagate. Thus, at large times, non-Boussinesq effects are such that the internal waves gradually build up (TOLSTOY, 1973) and eventually these internal waves separate into two components which, in the limit of large time, are identified as gravity waves and buoyancy oscillations. Buoyancy oscillations in this case are waves which, unlike gravity waves, consist of both propagating and evanescent internal waves, the later decaying exponentially in time. For large times, the gravity and buoyancy waves split and increasingly separate and eventually lose their non-Boussinesq character. In this limit, the Boussinesq gravity waves are (approximately) plane propagating internal waves of frequency $N|\cos\theta|$ and wavelength $2\pi r / Nt\sin\theta$. On the other hand, the Boussinesq buoyancy waves are radial oscillations of frequency N and are present everywhere in the fluid with a wavevector that is horizontal. In the non-Boussinesq far-field ($\beta r >> 1$), VOISIN (1991) has shown that a vertical point force (F_0) at the ground level generates a pressure field which decays as r^{-2} and is proportional to F_0.

Numerical Modeling of Non-Linear Atmospheric and Ionospheric Flows and Waves

The set of non-linear partial differential equations governing the atmospheric flows are converted to a corresponding set of finite difference equations in order to perform explicit computer integration in time and space. By examining exact solutions to linear and non-linear partial differential equations and their corresponding difference equations, two rules of modeling have been formulated (MICKENS, 1988). In order to prevent "ghost" solutions (numerical instabilities), the first rule is that the order of the finite-difference scheme should be equal to the order of the differential equation. The second rule applies to non-linear components of the differential equation and requires such non-linear terms to be treated non-locally on the lattice for stability (MICKENS, 1988).

For example, the difference equation used for the velocity equation in the x direction can be formulated as:

$$\frac{\partial u}{\partial t} + u\frac{\partial u}{\partial x} = -v\cdot\frac{\partial u}{\partial y} - w\frac{\partial u}{\partial z} + F \tag{21}$$

where F represents the remaining terms on the right-hand side of the x component of eq: (11). Upwind differencing is used for first order spatial gradients in the corresponding difference equation. However, where the velocity operates on its own velocity gradient, such non-linear terms are treated non-locally in a fashion similar to that which is necessary when integrating the Korteweg-deVries equation for multiple soliton solutions (CRANDALL, 1991). The difference equation for (21) is thus:

$$\frac{u_{ijk}^{n+1} - u_{ijk}^{n}}{\Delta t} + u_{ijk}^{n+1}\frac{u_{ijk}^{n} - u_{i-1jk}^{n}}{\Delta x} = -v_{ijk}^{n}\frac{u_{ijk}^{n} - u_{ij-1k}^{n}}{\Delta y} - w_{ijk}^{n}\frac{u_{ijk}^{n} - u_{ijk-1}^{n}}{\Delta z} + F_{ijk}^{n} \tag{22}$$

Hence, the new value of the velocity component, u, multiplies the x component of the spatial gradient composed of old u values, and so results in a non-linear integration algorithm given by:

$$u_{ijk}^{n+1} = \frac{u_{ijk}^{n} - v_{ijk}^{n}(u_{ijk}^{n} - u_{ij-1k}^{n})\frac{\Delta t}{\Delta y} - w_{ijk}^{n}(u_{ijk}^{n} - u_{ijk-1}^{n})\frac{\Delta t}{\Delta z} + \Delta t F_{ijk}^{n}}{1 + (u_{ijk}^{n} - u_{i-1jk}^{n})\Delta t / \Delta x} \tag{23}$$

Because we are computing density changes rather than the density itself, which is always positive, it is not necessary to use an algorithm which keeps the density from going negative, a restriction which can cause much difficulty (ORAN and BORIS, 1987). The updated variable is projected not from just the old dependent variable, a process that is inherently unstable, but from a distributed smoothed average of the variable at locations surrounding the specific spatial location. Such a smoothing method brings stability to the differencing scheme. However, the attendant numerical diffusion is minimized through anti-diffusion techniques (ORAN and BORIS, 1987) incorporated into the integration algorithm.

The second order derivatives in the viscosity and thermal conductivity terms are also modeled by finite differences taken at the surrounding spatial locations. In the explicit integration scheme, the updated flow velocities, temperature and density perturbations are obtained via their continuity equations, while the updated pressure perturbation is obtained from insertion of the updated density and temperature into the ideal gas equation.

Aside from the various differential equations, there are at least three boundary conditions important to the modeling of fluid flows. At the bottom boundary a vertical velocity variation along the boundary is prescribed by the seismic wave field, as previously discussed. (Because of the presence of a lower boundary layer above a complex topography, horizontal velocities are not constrained to be zero but, instead, constant velocity and density gradients are assumed in the vertical direction.) On the other hand, the topmost boundary should mimic the conditions for an open atmosphere, with specific considerations for buoyancy and field gradients. We have examined various options including fixing velocities, densities and their gradients. In the end, after many tests, we have adopted a general open flow boundary condition, which we also use for the artificial side boundaries, where all normal gradients are constant at these boundaries. However, if applied to the temperature variable, this would not permit heat flow through the open boundary. Therefore, for temperature, the second-order normal derivative is made constant.

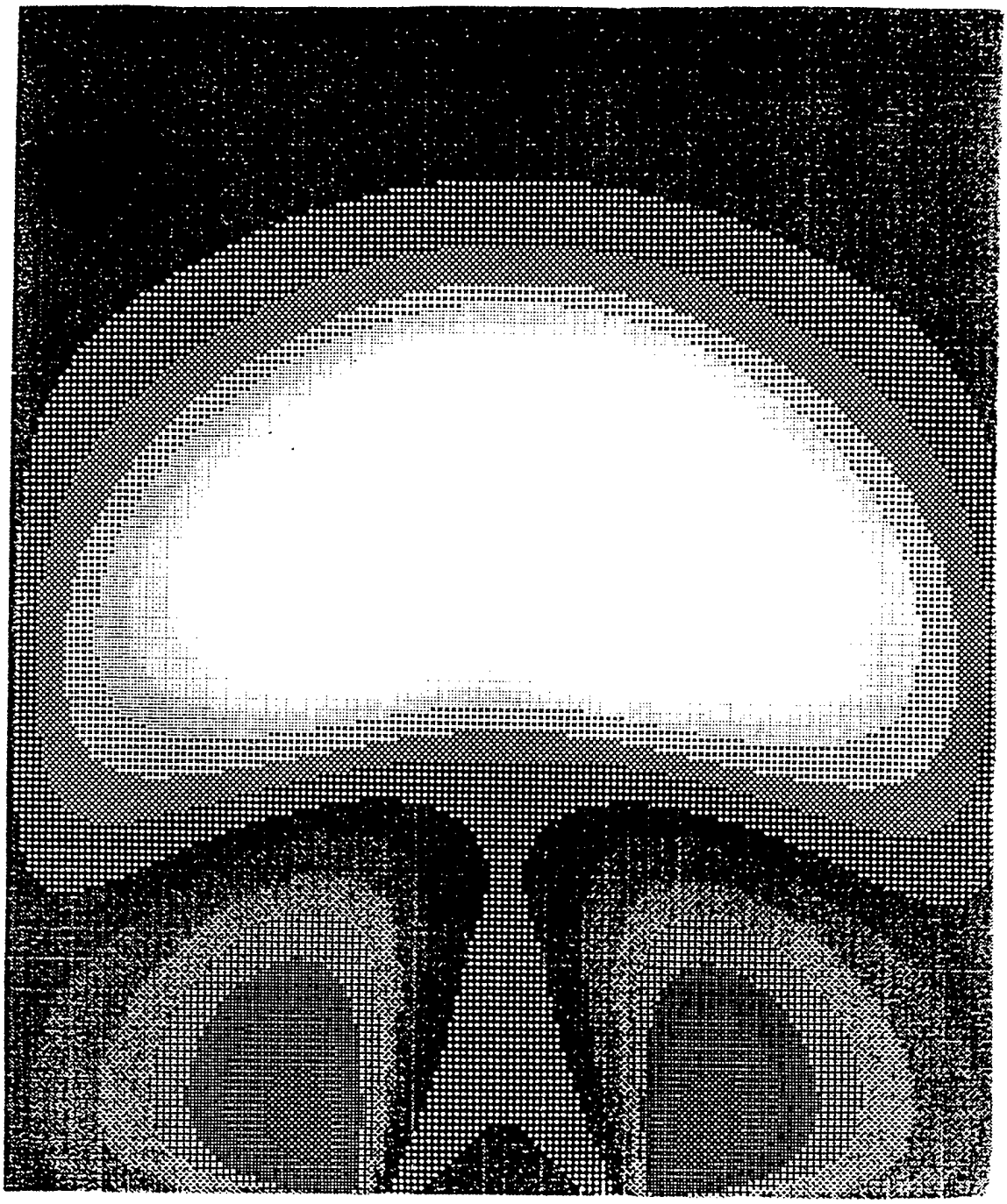

Figure 1. Cylindrically symmetric two-dimensional solution for the pressure field due to a constant velocity air source at the base of the atmosphere.

In general, a sufficiently large source near the surface will cause vertical velocity and density variations in the atmosphere which move upward and are initially observed as vortex ring thermals. Here, the full non-linear equations are needed, since the advective terms become of importance inside this vortex ring (TURNER, 1973). Experiments (SCORER, 1957) show that a vortex-like circulation is superimposed on the initial general vertical motion during the expansion period of the thermal, whose shape is slightly oblate spheroidal. Mixing takes place with the fluid ahead of the advancing front of the thermal and, as a result, the volume of the thermal continuously grows but the velocity eventually decreases.

Numerical simulations predicting the motion and structure of these thermals can be used as a test of modeling accuracy. In this regard, a vertical cross-section of a typical example is shown in Figure 1. As a function of time the transients propagate upward, with advective motion occurring both vertically and horizontally. A sequence of spiral circulation patterns develops through asymmetric screw modes across the horizontal cross-section, as previously argued by NYGREN et al. (1984), and energy and momentum are circulated through the plume by traveling waves through the circulation pattern, as seen by WEIL (1988). Similar effects have been observed in the real atmosphere when thermals and plumes propagate upward with similar asymmetric shearing flows (KUETTNER et al. 1987). At the neutral altitude, the buoyancy is zero in a density decreasing atmosphere, and these thermals break down into internal gravity waves through oscillations around the neutral elevation. Consequently, the non-linear modeling approach used here produces results that agree with observations and with results of other lines of analysis as well.

Seismic Source Effects

We are concerned with a variety of near-surface seismic sources that produce varying degrees of movement of the earth-atmosphere boundary which, in turn, result in the excitation of atmospheric disturbances. In particular, earthquakes can produce large, near-field, displacements of the surface of the earth surrounding the epicenter of the event.

Further, shallow earthquakes excite high-amplitude surface waves which propagate to large distances. Because of the large surface displacements associated with these waves and the near-source boundary movements, low-frequency disturbances in the atmosphere are produced which are quite large.

Underground nuclear explosions also produce a piston-like motion of the earth's surface directly above the source as well as large seismic surface waves at larger distances. Specifically, tamped nuclear explosions, with the device in near proximity to the surrounding rock, produce high particle velocities at the surface boundary and strong atmospheric coupling while "decoupled" explosions, which are detonated in large cavities, produce much lower boundary velocities and little atmospheric effects. Chemical explosions, for industrial purposes, produce large surface motions even when the yield is small since they are so near the surface.

Therefore, all seismic sources produce surface motions, with the vertical velocity component of the boundary surface acting as a piston on the local atmosphere. In this case compressive motions decrease the buoyancy of the local atmosphere while downward surface motions expand the local atmosphere and thereby produce increased buoyancy. In order to model these sources in numerical codes, it is necessary to model the time dependent particle velocity and stress at the free surface of the earth in the vicinity of the source epicenter. As indicated in eq: (15), the boundary conditions require continuity of the velocity component normal to the surface and continuity of the tractions at the surface. Consistent with the usual seismic theory approximations, the shear tractions in the atmosphere are taken to be negligible. Likewise, the pressure fluctuations in the atmosphere due to dynamic traction variations in the solid are taken to be of second order relative to the pressure variations caused by the seismically driven vertical movements of the air-solid boundary. Thus, the traction continuity requirement is automatically satisfied, to first order at least, and the remaining condition that produces first order coupling effects in the atmosphere is that given by the continuity of the normal component of particle velocity at the boundary.

Earthquakes produce large concentrated movements along linear faults with lengths which typically extend from tens to hundreds of kilometers for moderate to very large events. Near epicenters and near the fault trace of shallow earthquakes, ground surface accelerations significantly greater than the acceleration of gravity at the surface are commonly observed. Thus, there is the potential for large boundary velocities and strong atmospheric coupling.

In this regard, strike-slip faulting will produce no vertical motions at a flat free surface, but when appreciable topography exists such motions can initiate upward flows and waves in the atmosphere. On the other hand, shallow dip-slip and thrust faulting always will produce large vertical motions of the earth's surface, with opposite sides of the fault moving in opposite directions. Thus, earthquakes, even at depths that produce no surface breaks, can produce appreciable near-field surface velocities and significant static surface displacements close to the epicenter, as well as large low-frequency surface waves propagating thousands of kilometers from the source. Both near-source boundary movements and the far field surface waves have been observed to excite atmospheric waves (DAVIES and BAKER, 1965).

Large mining explosions also produce boundary movements with an areal-temporal distribution; in this case caused by ripple firing and the finite time delay between the sequence of separate explosions that are commonly used. These can be approximately modeled by using a sequence of discrete explosions, separated in time and space, followed by superposition of the single-source surface effects. Further, many large mining explosions not only produce large surface velocities, but also cause fracturing and eject gas and dust into the atmosphere. These ejecta produce mass coupling to the atmosphere and subsequent air flows and waves as well.

Underground nuclear test explosions, which are usually deeply buried so as to avoid surface fracturing and gas venting, produce a nearly spherical shock wave with a surface interaction that is roughly symmetric. The compressional wave from this source produces an upward vertical motion followed by a downward motion. Depending on the size of the

nuclear yield, its depth and the degree of coupling with the surrounding rock, the surface boundary can experience accelerations well over 1g. Because of the amplitude of the acceleration at the surface, the surface movement is usually complicated by the occurrence of spallation (separation of the rock along bedding planes), so that several peaks in the ground acceleration occur. In any case, the peak vertical velocity of the surface directly above the source can vary from hundreds of meters per second, for the largest tamped explosions, down to less than a meter per second, for small decoupled explosions detonated at moderate depths.

Since our purpose is to investigate the major consequences of the boundary movements produced by these sources, we will focus on estimating the amplitudes and time-dependent wave-form characteristics of the gravity waves that may be excited. In particular, we seek to determine whether the predicted amplitudes and wave characteristics imply effects that are easily measurable and can be used, along with seismic signal data, to distinguish between different source types, particularly between the different explosion types.

Qualitative differences in the relative amplitudes of seismic and gravity waves produced by the different seismic sources are indicated in Table 1. The seismic wave amplitude differences listed are based on theoretical and observational results (*e.g.* EVERNDEN *et al.*, 1987), while those for the gravity wave amplitudes are based on inferences from the limited observations and deductions from first order theoretical considerations. For example, in Table 1 we infer small to moderate amplitude gravity wave signals, in the 5 to 6 minute period range, for thrust and normal earthquakes. This inference is based on the GPS measurements, obtained by Calis and Minster (1995), following the rather large Northridge Earthquake. On the other hand, only very small gravity wave signals are expected for strike-slip earthquakes because of the small vertical movements to be expected at the atmosphere boundary. Likewise, as noted earlier, large atmospheric effects have been observed for near surface chemical explosions while the atmospheric effects from more deeply buried explosions, such as underground nuclear tests, will be reduced through propagation of signals

Table 1 - Qualitative gravity wave and seismic signal excitation levels relative to different types of seismic sources. Small sources of the same body wave magnitude (m_b) are compared, with $m_b \simeq 3$ assumed.

Discriminatory Signal Types	Seismic Source Types				
	Tamped Nuclear	Decoupled Nuclear	Industrial/Chemical Explosions	Shallow (Crustal Strike Slip Faulting	Shallow (Crustal) Normal Thrust
Atmospheric/ Ionospheric Gravity Wave	Moderate Amplitude (M)	Very Small (Undetectable) Amplitude (U)	Large Amplitude (L)	Very Small (Undetectable) Amplitude (U)	Moderate (S/M)
High Frequency Compressional Seismic Wave (f >10 HZ)	Moderate Amplitude (M)	Large Amplitude (L)	Moderate Amplitude (M)	Small Amplitude (S)	Small to Moderate (M)
Low Frequency Seismic Surface Waves	Moderate Amplitude (M)	Small Amplitude (S)	Moderate Amplitude (M)	Large Amplitude (L)	Large Amplitude (L)
Event "Signatures"	(M,M,M)	(U,L,S)	(L,M,M)	(U,S,L)	(M,S/M,L)

to the surface, as well as by the possible partial decoupling of the explosion from the medium around the source origin, including that achieved through use of a large cavity at the detonation point. More quantitative and precise results than those given in Table 1 should be obtained from the successful application of a non-linear numerical modeling approach and a well defined observational program. Therefore, at this stage, we hope to establish a more quantitative basis for source identification through a well-developed predictive capability.

In regard to modeling the atmospheric excitation by seismic sources, we only require the specification of the particle velocity produced by seismic waves at the earth-atmosphere interface in order to express the coupling of the seismic source to atmospheric flow and wave excitation via eq: (15). The general form of the seismic particle velocity at the earth's surface due to a shallow seismic source is, to first order, described by a maximum velocity level near the source epicenter, and along the strike of the fault in the case of an earthquake, with rapid, near exponential, fall-off in directions away from the fault line and the epicenteral zone. The time history of the normal component of the boundary velocity can also be approximated by a simple functional variation, where we expect either upward movement followed by a downward rebound, or the reverse in the case of some earthquake sources. Of course, in all cases there will be local deviations from this uniform, first order, boundary velocity variation due to medium heterogeneities and anisotropic characteristics, as well as from surface asymmetries and non-linearities. However, these variations are of short-wavelength spatially and of high frequency temporally. They are therefore averaged out during the excitation of the relatively low frequency, long wavelength gravity waves; so that in modeling gravity wave excitation the first order long wavelength approximation of the lower atmosphere boundary velocity movement is adequate.

The previous considerations suggest that a good first order approximation to the boundary velocity can be obtained by taking the normal component of the seismic particle

velocity to be of Gaussian form on the surface (S_0) which we take to be the plane $X_3 = 0$. In particular, on S_0:

$$v_n = D_0 \prod_{i=1}^{2} \exp\left[-\left(\frac{x_i - \bar{x}_i}{\Delta x_i}\right)^2\right] \frac{d}{dt} \exp\left[-\left(\frac{t-\bar{t}}{\Delta t}\right)^2\right]$$

with v_n denoting the solid medium particle velocity normal to S_0 and $\bar{x}_i$, i = 1,2 and $\bar{t}$ being the epicenteral coordinates of the source and the origin time, respectively. Here also Δx_i (with i = 1,2) and Δt are the Gaussian scale factors for the spatial and temporal time variations. The parameter D_0 is the (positive) magnitude of the maximum dynamic surface displacement. Taking the time derivative and applying the continuity condition for the particle velocities across S_0, with w denoting the vertical component of the particle velocity in air at S_0, we have

$$w(x_i, x_2, o, t) = -\frac{2D_o}{\Delta t}\left(\frac{t-\bar{t}}{\Delta t}\right) \exp\left[-\left(\frac{t-\bar{t}}{\Delta t}\right)^2\right] \prod_{i=1}^{2} \exp\left[-\left(\frac{x_i - \bar{x}_i}{\Delta x_i}\right)^2\right] \qquad (22)$$

This expression contains enough flexibility to provide first order representations of the boundary velocity in the near field for all the seismic sources of interest, since the spatial scale factors Δx_1 and Δx_2 can be chosen differently and the surface velocity variations for the different source geometries can all be well represented.

Typical values of the parameters Δx_i for small to moderate earthquakes are in the range from about 1 to 5 km. These choices for the spatial parameters are roughly appropriate to earthquakes with magnitudes in the range from about 3 to 5. The time parameter Δt is proportional to the dominant period of the particle velocity variation at the surface; specifically it is about one-fourth of the period. In this near field distance range an appropriate range for Δt can be obtained from observations of the dominant frequency of near field seismic waves for shallow sources, with depths less than 5 km. For explosions in the 3 to 5 magnitude range the dominant frequencies are from about 25 to 5 HZ, respectively (EVERENDEN *et al.*, 1987). Thus, the appropriate Δt range is from about 0.1 to .05. For

earthquakes in the same magnitude range the dominant seismic signal frequencies are somewhat lower, so that the appropriate range for Δt is from about .05 to .25 sec.

Based on observations of accelerations greater than 1 g at the surface for shallow moderate sized earthquakes, along with the associated measurements of peak velocities that range up to several tens of meters per second, we infer that the displacement parameter D_0 appearing in (24) should have a range of from about .5 m to about 2.5 m for shallow earthquakes with magnitudes ranging from 3 to 5. For underground explosions, however, the signal frequencies are higher and D_0 values are lower (.1 m to .5 m) for this magnitude range. These values of D_0 are also consistent with observations.

Therefore, the first order representation in (24) using the various parametric values indicated above, can be made consistent with average near-field seismic observations from small to moderate earthquakes and exlosions and should provide good first order estimates for the boundary velocity variations. The examples given in the next section will be representative of the excitation of low frequency atmospheric gravity waves by seismic events in the interesting magnitude range from 3 to 5. For this purpose we will use an earthquake near magnitude 4 and use a maximum value of about 4 m/sec for w, with Δt = .1 sec. (so D_0 = .2 m) and with $\Delta x_1 = 2\Delta x_2 = 4$ km. These parameters are roughly appropriate for an earthquake of magnitude 4 at a depth of about 5 km. For shallower depths the values of w and D_0 increase. At a depth of 1 km the maximum value for w would be near 50 m/sec, with D_0 about 2 m.

Modeling of Gravity Waves and Associated Ionospheric Electron Density Variations

The boundary source represented in (24), with parameters as enumerated for a magnitude 4 earthquake, produces a compressive movement in the atmosphere followed by an expansion when the event has a thrust mechanism. The initial increased density from the compressive pulse in the atmosphere is propagated upward more slowly than the following dilatational pulse which has increased buoyancy due to reduced density. One also finds that

the time-dependent transient pulse in 3-dimensions has nonsymmetric flows that are critical to the upward motion of the buoyancy wave. In particular, as a function of time the transients propagate upward with advective motion occurring both vertically and horizontally and a sequence of spiral circulation patterns develops through asymmetric screw modes across the horizontal cross-section, as previously argued by NYGREN *et al.*, (1984). The circulation patterns across the vertical cross-section are characterized by upward central motions of the lighter matter, which, at the neutral buoyancy level, pushes outward to the side. Then, as the pulse centroid moves through this level the air mass is pulled back toward the center. The advected air mass therefore tries to remain in its horizontal stratification in order to minimize changes in its gravitational potential. Further, energy and momenta are circulated through the plume by traveling waves through the circulation pattern, as was also observed by WEIL (1988). These effects have been observed in the real atmosphere when thermals and plumes propagate upward with similar asymmetric shearing flows (KUETTNER *et al.*, 1987). We also observe that the pulse increases its horizontal wavelengths as time progresses, with 800 km wide grids insufficient to map the whole pulse structure at an altitude of 100 km.

Figure 2 shows the normalized horizontal velocity as a function of time and location along an axis through the grid, for this seismic source. The altitude of the flow is about 170 km and amplitude values are normalized to the velocity of sound. The flipping of the velocity direction in time is regular, with the change in direction along the axis occurring directly over the source. The flipping of the direction of flow velocity at sharp density gradients was predicted by the linear theory approximations for gravity waves (HINES, 1960,1974), and was confirmed numerically for two dimensional systems by GREENE and WHITAKER (1968) who found gravity waves forming at the 120 km altitude. Thus, it appears as if a source of thermospheric modes exists at this altitude (FRANCIS, 1975). The downward slanted direction of the phase propagation is readily observed, as predicted by the linear approach of HINES (1960). Figure 3 shows the behavior of the normalized perturbed

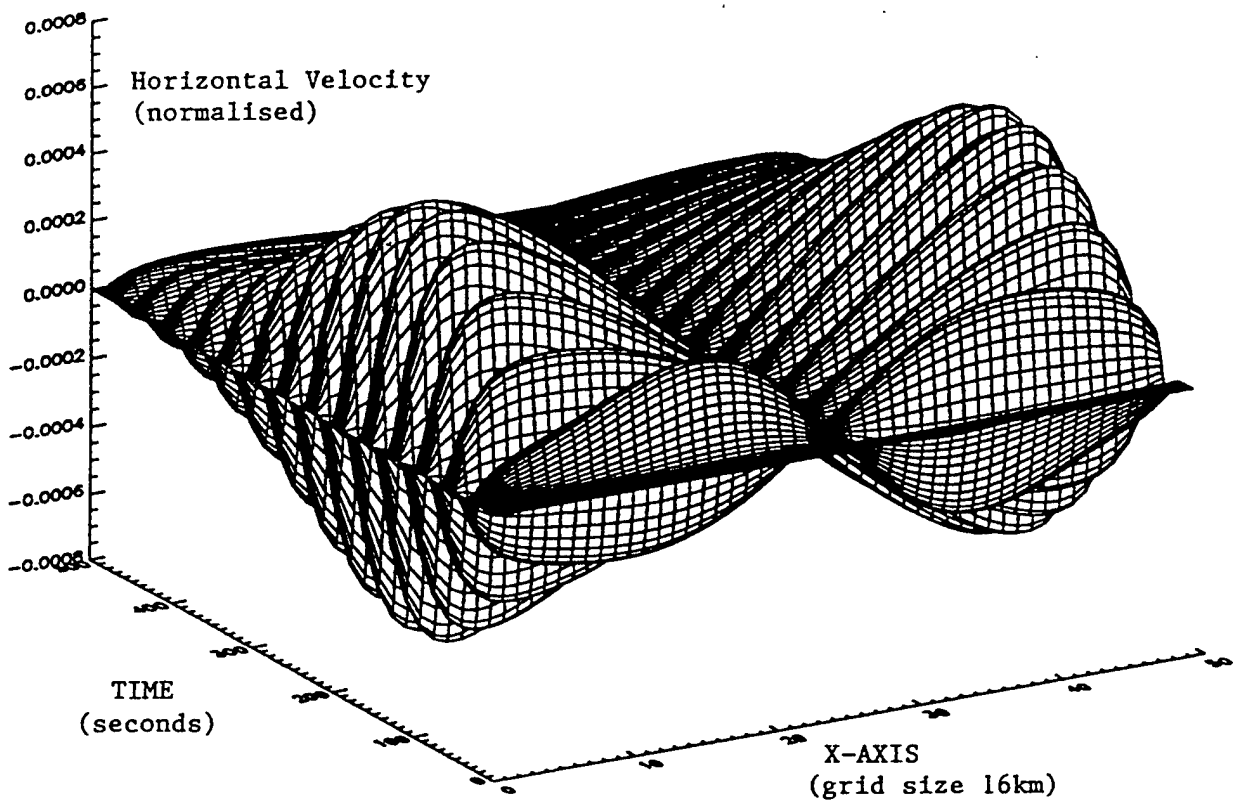

Figure 2. Normalized horizontal velocity, scaled by the surface air velocity of 3.4 m/sec, for a gravity wave as a function of time after its initial onset. The x component of the particle velocity at a height of 170 km above the surface is shown. The boundary source has a Gaussian spatial distribution, with $\Delta x_1 = 2\Delta x_2$ = 4 km. The boundary velocity time variation corresponds to the time derivative of Gaussian variation, with Δt = .1 sec. The maximum boundary velocity value is 4 m/sec. A dynamic drag coefficient of .01 for the atmosphere-ionosphere is assumed along with a choice of a numerical time step of .1 sec in the finite difference computation.

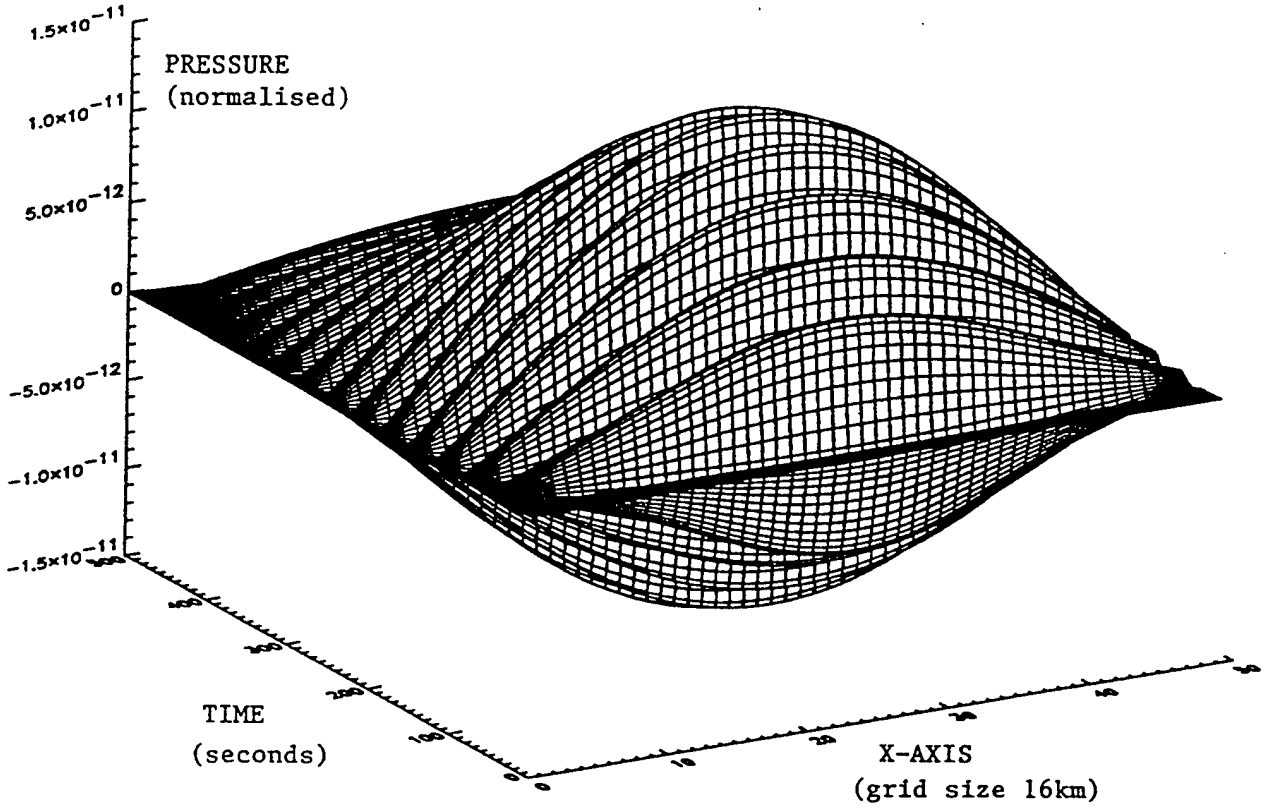

Figure 3. Normalized pressure (scaled by atmospheric pressure at the earth's surface) of a gravity wave as a function of time after initial onset. The source type and drag coefficient are identical to those for Figure 2, and the height is also at 170 km.

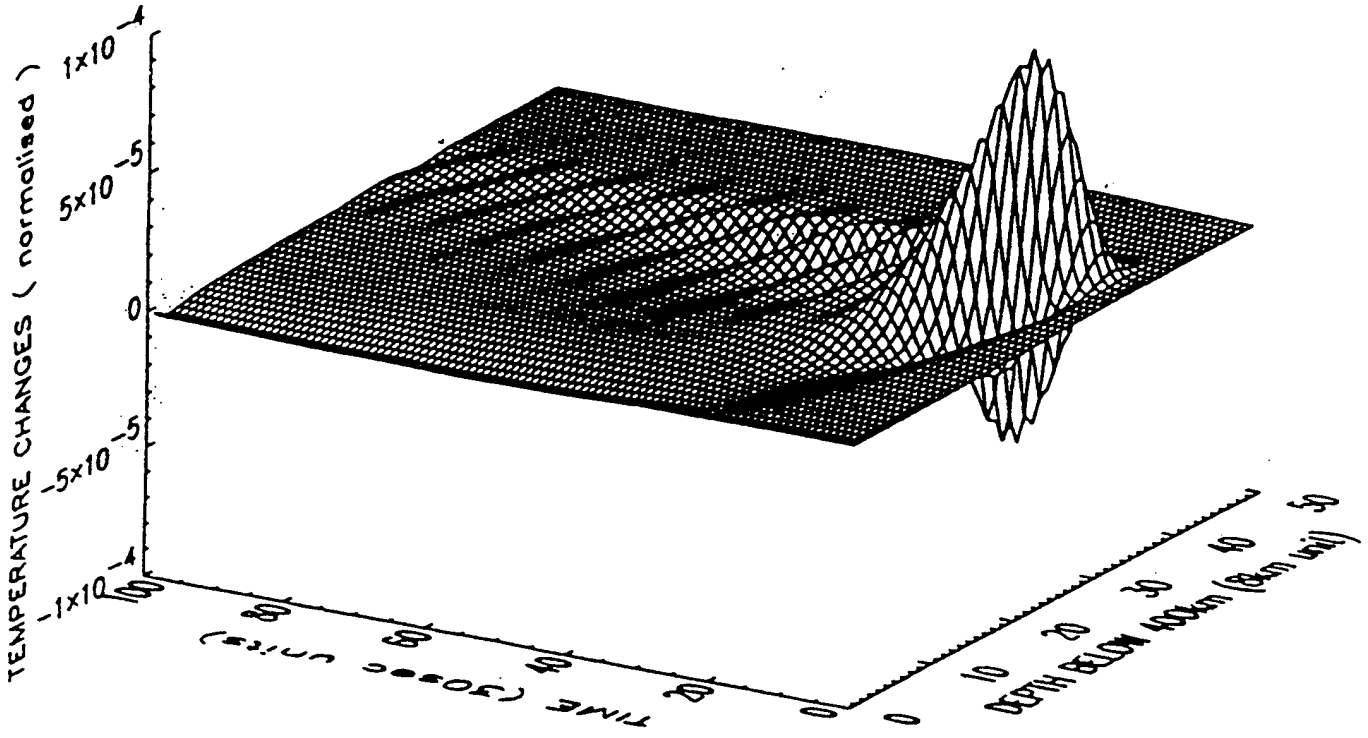

Figure 4. Normalized temperature (scaled by $T_0 = 288.16\,^{o}K$) for a gravity wave as a function of time after initial onset. The third axis shows depth below 400 km. The location is directly above a surface source of the same type as is described in Figure 2. The drag coefficient is the same as for the results shown in Figures 2 and 3.

pressure field under the same conditions as in Figure 2, with all these results being consistent with the earlier predictions from 2 D numerical modeling and the linear analytical estimates.

Figure 4 shows the temperature disturbance above the source as a function of time at different heights. An initial large pulse decays in amplitude with oscillations at about a 5 minute period. The gravity wave interacting with the steep gradients at the thermopause is thought to cause these leaky modes and their periods are seen to vary from 3 to 5 minutes, and includes the lowest orders of acoustic and gravity modes. Such oscillations have been recorded in numerous observations of waves produced by near surface sources (GEORGES, 1968) and in observations of ionosondes near Space Shuttle ascents (JACOBSON and CARLOS, 1994).

To first order, the electrons in the ionosphere are assumed to move with the flow of the dominant neutrals and the change in the electron density is calculated from the conservation law in equ: (17), where integration over time gives the total electron density variation. For the boundary velocity level used for the magnitude 4 earthquake we find changes in electron density that are somewhat less than one tenth of a percent. When the drag and dissipative effects are small, we obtain somewhat larger peak amplitudes and also find oscillations in the electron density changes that are induced by flipping of the gravity wave at the thermocline.

Figure 5 shows the electron density changes in time at various altitudes between 125 km and 250 km for the representative magnitude 4 earthquake source. These results show the characteristic oscillations imposed on the temporally and spatially complex pulse when the turbulent drag coefficient is small. When the dissipation is increased, these oscillations are not apparent. Further, the dissipative mechanisms can be adjusted to vary the decay of the pulse in time and with height.

Figure 6 compares the electron density variations in the ionosphere due to gravity waves from a source of the form used previously, with the same pulse duration but with different

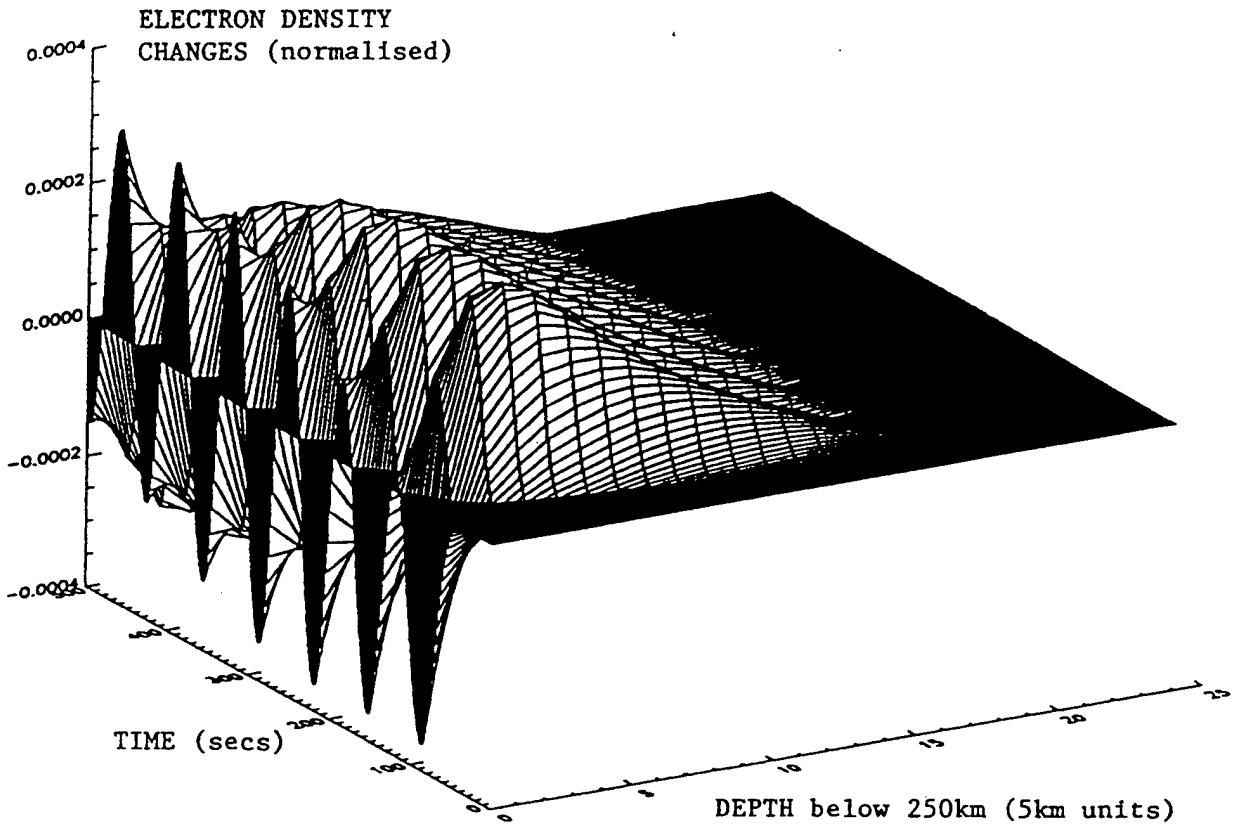

Figure 5. Electron density changes (normalized by $10^{12}/m^3$) after the onset of a gravity wave, for altitudes between 125 km and 250 km. The boundary velocity source is as in Figure 2. The dynamic drag coefficient is .001 in this example.

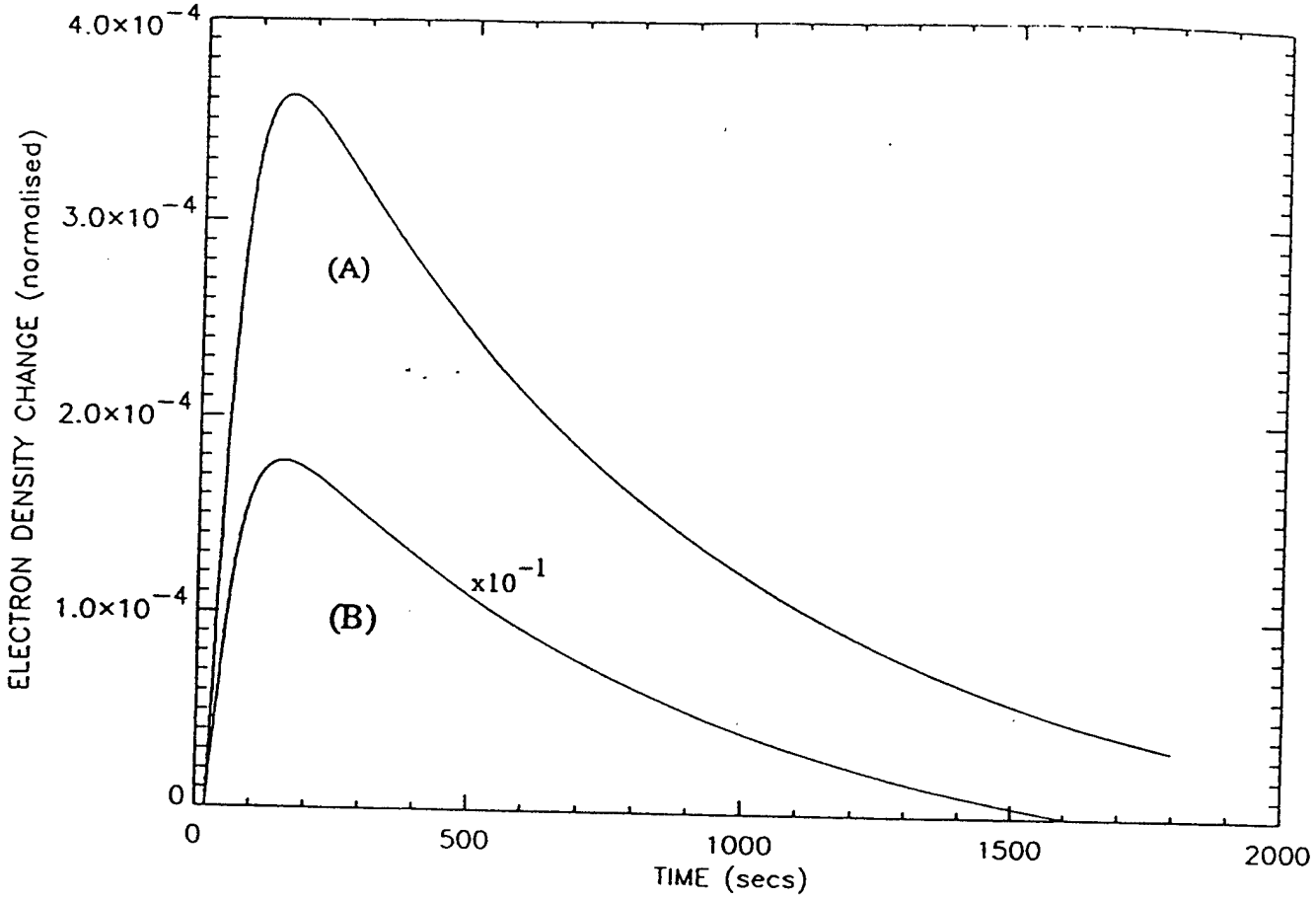

Figure 6. Normalized electron-density changes due to a gravity wave as a function of time after initial onset. Depth below 250 km is indicated on the third axis. The boundary velocity source has the same form as described in Figure 2, except that maximum velocity values are varied. The drag coefficient was taken to be .02. Case (A): The scale velocity for the source is 3 m/sec. Case (B): The source has a scale velocity of 15 m/sec. (The actual electron density change is 10 times the value on the scale for case B).

maximum boundary velocities appropriate to a shallower event. These simulations assumed a high dynamic drag coefficient of .02. The results have qualitative similarity in magnitude to observed electron density changes above near-surface sources (PIERCE et al., 1971, GOKHBERG, 1991) but lack oscillatory character due to the high drag coefficient assumed. Of course, if the drag coefficient is reduced oscillatory variations like that in Figure 5 are obtained, with amplitudes somewhat above those shown in Figure 6.

Comparisons of Modeling Results with Observed Electron Density Variations Inferred from GPS Data

On January 17, 1994, at 4:31 am local time, the Northridge earthquake occurred in southern California about 30 km north of the Los Angeles basin (HAUKSSON *et al.*, 1994). This magnitude 6.6 earthquake ruptured with a thrust mechanism of a 10 km long fault segment striking N120E and dipping 45° to the southwest (THIO and KANAMORI, 1994). The rupture started at a 19 km depth and propagated upward to a depth of about 5 km, but did not reach the surface (WALD and HEATON, 1994). This produced 40 cm of static vertical displacement directly above the fault plane (HUDNUT *et al*, 1994). Ground accelerations of more than 1.5 g were recorded 5 km from the epicenter (EGAL *et al.*, 1994).

The Northridge epicenter was located within the permanent network of GPS stations operating in southern California (PGGA network, BOCK *et al.*, 1993) and CALAIS and MINSTER (1995) used the GPS data from the PGGA network to estimate fluctuations of the ionospheric electron content at distances up to 1000 km from the source. Specifically, since the radio signals broadcast at 1.57542 GHz (f_1) and 1.2276 GHz (f_2) by GPS satellites are dispersively delayed along their path by interactions with free electrons in the ionosphere, so that the differential delay between the f_1 and f_2 frequencies is proportional to the electron density along the ray path (KLOCUBHAR, 1985), then measured phase delays can be used to calculate time dependent electron density variations. Therefore, using phase and P-code delays recorded on the two GPS frequencies, CALAIS and MINSTER made direct

measurements of the Total Electron Content (TEC) of the ionosphere, corresponding to the electron density integrated along the line of sight.

The TEC values along the signal paths at the GPS receiving stations were computed and then corrected to a "vertical electron content" (VEC) above the receivers in order to remove the geometric effect of the different satellite paths to the receivers. Since the power spectrum of the VEC variation is dominated by very low frequency components introduced by the solar cycle, it is necessary to filter out this large noise component in order to extract a signal corresponding to the electron density variations introduced by any gravity wave. Therefore, CALAIS and MINSTER band-pass filtered the VEC data in the period range from about 3 to 10 minutes, based on the modeling predictions shown in Figure 5.

The results of applying the simple band pass filtering to the GPS data at several receiver-satellite pairs near the earthquake epicenter (within 200 km or so) are shown in Figures 7 and 8. In Figure 7 a single (typical) recording of the VEC by a ground GPS receiver, covering the time frame from just before the earthquake until just after, is shown. A signal arriving shortly after the earthquake, with a signal to noise ratio of about 2 or slightly greater, can be seen in this record. This signal has a period of about 5 minutes and a time variation approximating that predicted in Figure 5. Naturally, because of the movement of the satellite there is some distortion of the VEC signal observed. Nevertheless, the agreement between prediction and observation is quite good in terms of wave form similarity and the predicted and observed dominant period.

Since there are many sources of ionospheric gravity waves, it could only be fortuitous that a larger signal above the noise level is seen shortly after the earthquake at a single GPS receiver. However, Figure 8 shows several receiver recordings, band pass filtered as in Figure 7, that all show a signal above the background level arriving at different times after the earthquake. In fact, since the records are arranged with distance of the receiver-satellite signal path from the event epicenter, which increases from the bottom to the top of the record section shown, it can be seen that the VEC signal has a move out (variable time

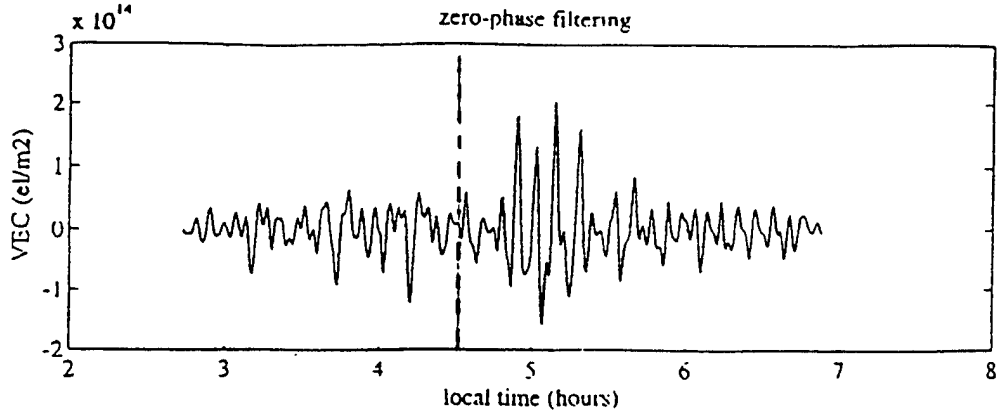

Figure 7 Pass-Band Filtered (3-10 minute period range) VEC time recording for a single satellite-receiver pair (site MATH, satellite 13). The dashed line indicates the origin time of the earthquake (magnitude 6.6,). A signal, above background by about a factor of 2, is detected with onset between 4:30 to 5:00 local time. (Figure from Calais and Minster, 1994)

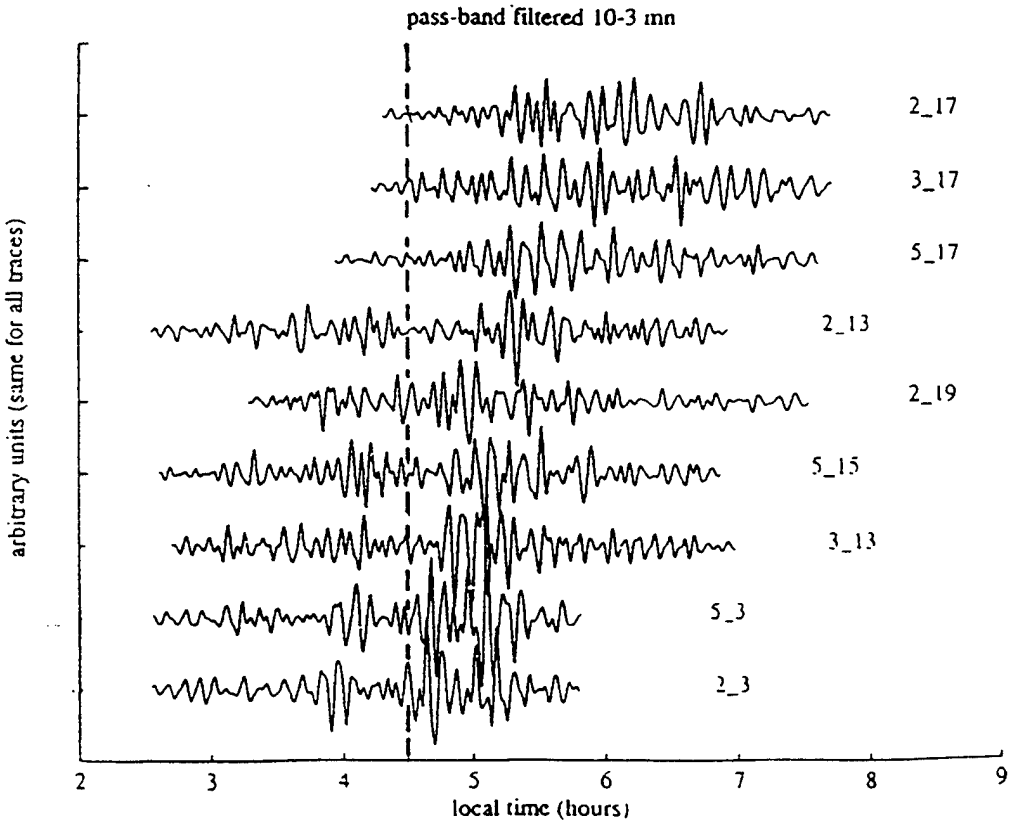

Figure 8 Observed filtered VEC recordings at a number of receiver-satellite pairs. The recordings are ordered by increasing distance of the signal path from the epicenter, with the closest at the bottom. The dotted line shows the earthquake origin time and the numbers to the right indicate receiver-satellite pairs for each recording. All the recordings show evidence of a signal, with a time delay of its onset increasing with increasing distance of the receiver-satellite path from the event epicenter, as would be expected for a slowly moving ionospheric gravity wave perturbation of the electron density. (Figure from Calais and Minster, 1994)

delay) that increases with distance. This, of course, would be expected for an ionospheric electron density perturbation arising from a gravity wave source near the epicenter of the earthquake. The propagation speed indicated by this sequence of signal time delays is between 300 and 600 m/sec, a range consistent with gravity wave speeds in the ionosphere. Furthermore, the initiation of the disturbance has a delay time consistent with the earthquake excitation of gravity waves near the epicenter at the time of the event. Therefore, there is little doubt that the perturbations in the electron density along all the signal paths are due to propagating gravity waves which excited by this earthquake.

A somewhat more complete comparison of the observations and the modeling predictions can be made using previous modeling results. Of course the magnitude 4 earthquake assumed in the computations for the results in Figure 5 is quite different than the Northridge earthquake, which was of larger magnitude (6.6) and was deeper, with a hypocentral depth of about 19 km. However, adjusting for the depth differences as well as the effects of the magnitude differences between the events, indicates that the Northridge event would have a boundary velocity about as large as that for the shallower "standard" earthquake, but with values of Δx_i somewhat larger than those used for the representative magnitude 4 earthquake. Thus, the Northridge earthquake would be expected to produce somewhat larger atmospheric gravity waves, but of the same order of magnitude. This estimate, in fact, is consistent with the maximum VEC predicted by the results in Figure 5. That is, the maximum unnormalized electron density variation from the predictions is approximately $(3 \times 10^{-4}) \times 10^{12}$ el/m^3, or 3×10^8 el/m^3. Converted to a VEC variation by simply multiplying by the thickness (h) of the ionosphere, gives about 3×10^{14} el/m^2. The value observed for the Northridge earthquake is (coincidentally) very close to this value.

Of course these comparisons are quite crude, since there has been no systematic effort to vary atmospheric dissipation in the modeling in order to match the dominant period of the observed gravity waves, and the source differences are only roughly estimated. Nevertheless, the rough agreement with the predictions from a "standard" earthquake is

significant, and there can be little doubt that relatively minor adjustments to the atmospheric-ionospheric dissipation parameters, as well as to source boundary velocity parameters, could produce quite detailed fits to the observations.

SUMMARY AND CONCLUSIONS

Non-linear numerical modeling in 3-D has been used to investigate the excitation of atmospheric and ionospheric disturbances due to shallow (upper crustal) seismic sources. Grid zones as large as 800 by 800 kilometers in area and 400 km n altitude were used with grid dimensions between 2 and 15 km also used. The modeling employs non-local differencing for the non-linear terms in the equations and results in a non-linear integration algorithm that is found to be essential for accuracy and stability. Altitude dependent wave dissipation effects, such as arise from interaction of the gravity waves with background wind turbulence, are modeled using a drag force proportional to the negative of the wave particle velocity. Predictions of gravity wave characteristics are found to be very sensitive to the magnitude of the dynamic drag coefficient, with oscillatory gravity waves occurring all the way into the ionosphere for values below .01. For a larger average drag coefficient the waves are over damped and oscillations are absent.

Results from numerical simulations agree with predictions from linear theory approximations and also show non-linear characteristics that have been observed experimentally. A comparison of model predictions of electron density fluctuations due to earthquake generated atmospheric gravity waves with observations of the variations in the Vertical Electron Concentration (VEC) obtained from GPS receivers after the Northridge earthquake in California showed agreement in the oscillatory wave form and dominant (near 5 minutes) period of the oscillations. In addition, the amplitude levels of the observations and predictions were consistent with each other. The agreement with observations implies that a low value for the average dynamic drag coefficient is appropriate and that small to moderate shallow earthquakes, of thrust or normal type, will produce gravity waves of

sufficient amplitude to be detectable through the perturbations they cause in the ionospheric electron density. Additionally, GPS satellites and receivers provide a ready made network for such measurements using the approach followed by CALAIS and MINSTER (1995) in their study of the signals from the Northridge earthquake.

The opportunity to use GPS observations and the non-linear modeling capability to study atmosphere and ionosphere properties seems evident since there would appear to be an abundance o shallow seismic sources which can excite gravity waves producing measurable effects. In particular shallow, upper crustal thrust and normal earthquakes, volcanic eruptions, large subsurface (chemical and nuclear) explosions, as well as much smaller chemical explosions at the surface, should all produce measurable effects. Further, it should be possible to use the electromagnetic sounding measurements, along with seismic measurements, to differentiate between these various seismic sources. Therefore, a dual field sensing approach, involving GPS and seismic field sensors, could be used to better distinguish between large industrial explosions and underground nuclear tests, particularly tests producing signals that have been reduced by decoupling techniques.

ACKNOWLEDGMENTS

This research was supported by the United States Air Force contract F19628-90–K-0051.

REFERENCES

BAKER, D.M., and K. DAVIES, Waves in the ionosphere produced by nuclear explosions, *J. Geophys. Res.* 73, 448-451, 1968.

BARCILON, V., and N. BLEISTEIN, Scattering of inertial waves in a rotating fluid, *Stud. Appl. Math.* 48, 91-104, 1969.

BATCHELOR, G.K., An *Introduction to Fluid Dynamics, Cambridge* University Press, England, 1967.

BEYNON, W.J.G., and E.S.O. JONES, Ionospheric effects of nuclear explosions, *Nature* 196, 253-254, 1962.

BLANC, E., Observations in the upper atmosphere of infrasonic waves from natural or artificial sources: A summary, *Annales Geophysicae* 3, 6, 673-688, 1985.

BLANC, E., and D. RICKEL, Nonlinear wave fronts and ionospheric irregularities observed by HF sounding over a powerful acoustic source, *Radio Science* 24, 3, 279-288, 1989.

BOCK, Y., D.C. AGNEW, P. FANG, J.F. GENRICH, B.H. HAGER, T.A. HERRING, K.W. HUDNUT, R.W. KING, S. LARSEN, J.B. MINSTER, K. STARK, S. WDOWINSKI, and F.K. WYATT, Detection of crustal deformation from the Landers earthquake sequence using continuous geodetic measurements, *Nature* 361, 337-361, 1993.

CALAIS, E., and J.B. MINSTER, GPS detection of ionospheric perturbations following the Jan 17, 1994, Northridge earthquake. *Geop. Res. Let.* 22, 1045-1048, 1995.

DAVIES, K., and D.M. BAKER, Ionospheric effects observed around the time of the Alaskan Earthquake of March 28, 1964, *J. Geophys. Res.* 70, 2251-2254, 1965.

DEARDORFF, J.W., Sub-Grid-Scale Turbulence Modeling, *Advances in Geophysics* 28, 337-344, 1985.

DICKINSON, R.E., Propagators of atmospheric motions, *Rev. Geophysics* 7, 483-514, 1969.

EGAN, J.A., F.I. MAKDISI, and D. ROSIDI, Near-field vertical ground motions from the 17 January 1994 Northridge earthquake: were they unusual? *Seismological Research Letters* 65, 1, 1994.

EVERNDEN, J.F., C.B. ARCHAMBEAU and E. CRANSWICK, An Evaluation of Seismic Decoupling and Underground Nuclear Test Monitoring using High-Frequency Seismic Data, *Rev. Geophysics* 24, 143-215, 1986.

FRANCIS, S.H., Global Propagation of Atmospheric Gravity Waves: A Review, *J. Atmos. Terr. Phys.* 37, 1011-1054, 1975.

FRIEDMANN, J.P., Propagation of internal gravity waves in a thermally stratified atmosphere, *J. Geophys. Res.* 71, 1033-1054, 1966.

GARDNER, C.S., Introduction to ALOHA/ANLC-93: The 1993 airborne lidar and observations of the Hawaiian airflow/airborne noctilucent cloud campaigns, *Geop. Res. Let.* 22, 2789-2792, 1995.

GEORGES, T.M., Short-period ionospheric oscillations associated with severe weather, in *Acoustic Gravity Waves in the Atmosphere* 171-178, (ed. by T.M. GEORGES), E.S.S.A. Symposium, U.S. Govt. Printing Office, Washington, D.C., 1968.

GOKHBERG, M.B. *et al.,* Electromagnetic effects of nuclear underground explosions and possibilities of non-seismic verification methods, Internal Report, Institute of Physics of the Earth, Moscow, 1990.

GREENE, J.S., and W.A. WHITAKER, Theoretical calculations of traveling ionospheric disturbances generated by low-altitude nuclear explosions, in *Acoustic Gravity Waves in the Atmosphere* 45-64, (ed. by T.M. GEORGES), E.S.S.A. Symposium, U.S. Govt. Printing Office, Washington, D.C., 1968.

HARKRIDER, D.G., Theoretical and observed acoustic-gravity waves from explosive sources in the atmosphere, *J. Geophys. Res.* 69, 5295-5321, 1964.

HAUKSSON, E., K. HUTTON, H. KANAMORI, L. JONES, and J. MORI, The M_W6.7 Northridge, California, Earthquake of January 17, 1994 and its aftershocks, *Seismological Research Letters* 65, 1, 1994.

HINES, C.O., Internal atmospheric gravity waves at ionospheric heights, *Can. J. Phys.* 38, 1441-1481, 1960.

HINES, C.O., The Upper Atmosphere in Motion, *Geophysical Monograph 18*, Am. Geophys. Union, Washington, D.C., 1974.

HUDNUT, K.W., M.H. MURRAY, A. DONNELAN, Y. BOCK, P. FANG, M. CLINE, Y. FENG, Z. SHEN, B. HAGER, T. HERRING, and R. KING,

Coseismic displacements of the 1994 Northridge, California, earthquake, *Seismological Research Letters* 65, 1, 1994.

IMAMURA, T., and T. OGAWA, Radiative damping of gravity waves in the terrestrial planetary atmospheres, *Geop. Res. Let.* 22, 267-270, 1995.

JACOBSON, A.R., and R.C. CARLOS, Observations of acoustic-gravity waves in the thermosphere following Space Shuttle ascents, *J. Atmos. Terr. Phys.* 56, 4, 525-528, 1994.

JACOBSON, A.R., R.C. CARLOS, and E. BLANC, Observations of ionospheric disturbances following a 5-kt chemical explosion. 1. Persistent oscillation in the lower thermosphere after shock passage, *Radio Science* 23, 820-830, 1988.

KELLEY, M.C., and D.L. HYSELL, Equatorial spread-F and neutral atmospheric turbulence: a review and a comparative anatomy, *J. Atmos. Terr. Phys.* 53,8, 695-708, 1991.

KLOBUCHAR, J.A., Ionospheric time delay effects on earth-space propagation, *Handbook of Geophysics and The Space Environment*, edited by A.S. Jursa, Chap. 10.8, 1084-1088, U.S. Air Force, Washington D.C., 1985.

KLOSTERMYER, J. Nonlinear investigations of the spatial resonance effect in the nighttime equatorial F regions *J. Geophys. Res.* 83, 3753-3760, 1978.

KUETTNER, J.P., P.A. HILDEBRAND, and T.L. CLARK, Convection Waves: Observations of gravity wave systems over convectively active boundary layers, *Quart. J. Roy. Meteor. Soc.* 113, 445-467, 1987.

LIGHTHILL, M.J., *Waves in Fluids*, Cambridge University Press, England, 1988.

MANSON, A.H., Gravity Wave Horizontal and Vertical Wavelengths: An Update of Measurements in the Mesopause Region (80-100 km), *J. Atmos. Sciences* 47, 2765-2773, 1990.

MIESEN, R.H.M., Applying weakly nonlinear internal wave theories to solitary waves in the atmosphere, *J. Atmos. Terr. Phys.* 54, 314, 363-372, 1992.

MIESEN, R.H.M., P.C. DEJAGHER, L.P.J. KAMP, and F.W. STIUJTER, Damping of acoustic gravity waves caused by the conductivity of the ionosphere, *J. Geophys. Res.* 94, 16269-16275, 1989.

NYGREN, T. *et al.,* The role of electric field and neutral wind direction in the formation of sporadic E-layers, *J. Atmos. Terr. Phys.* 46, 4, 373-381, 1984.

PIERCE, A.D., J.W. POSEY, and E.F. ILLIF, Variation of nuclear explosion generated acoustic-gravity wave forms with burst height and with energy yield, *J. Geophys. Res.* 76, 21, 5025-5042, 1971.

PIERCE, A.D., Theoretical source models for the generation of acoustic-gravity waves by nuclear explosions, in *Acoustic Gravity Waves in the Atmosphere* 9-24, (ed. by T.M. GEORGES), E.S.S.A. Symposium, U.S. Govt. Printing Office, Washington, D.C., 1968.

PITTEWAY, M.L.V., and C.O. HINES, The viscous damping of atmospheric gravity waves, *Can. J. Phys.* 41, 1935-1948, 1963.

SCORER, R.S., Experiments on convection of isolated masses of buoyant fluid, *J. Fluid Mech.* 2, 583-594, 1957.

TOLSTOY, I., *Wave Propagation*, McGraw-Hill Press, New York, 1973.

TURNER, J.S., Buoyancy Effects in Fluids, Cambridge University Press, England, 1973.

VOISIN, B., Internal wave generation in uniformly stratified fluids, Green's function and point sources, *J. Fluid Mech.* 231, 439-480, 1991.

VOLLAND, H., *Atmospheric Tidal and Planetary Waves*, Kluwer Academic Pub., Boston, Mass., 1988.

WALD, D., and T. HEATON, A multidiscipliinary source analysis of the 1994 (M_W6.7) Northridge earthquake using strong motion, teleseismic, and geodetic data, *Seismological Research Letters* 65, 1, 1994.

WEIL, J.C., Plume Rise, in *Lectures on Air Pollution Modeling*, ed. by A. Venkataran and J.C. Wyngaard, Am. Met. Soc. Boston, 119-166, 1988.

THOMAS AHRENS
SEISMOLOGICAL LABORATORY 252-21
CALIFORNIA INSTITUTE OF TECHNOLOGY
PASADENA, CA 91125

SHELTON ALEXANDER
PENNSYLVANIA STATE UNIVERSITY
DEPARTMENT OF GEOSCIENCES
537 DEIKE BUILDING
UNIVERSITY PARK, PA 16801

RICHARD BARDZELL
ACIS
DCI/ACIS
WASHINGTON, DC 20505

DOUGLAS BAUMGARDT
ENSCO INC.
5400 PORT ROYAL ROAD
SPRINGFIELD, VA 22151

WILLIAM BENSON
NAS/COS
ROOM HA372
2001 WISCONSIN AVE. NW
WASHINGTON, DC 20007

ROBERT BLANDFORD
AFTAC
1300 N. 17TH STREET
SUITE 1450
ARLINGTON, VA 22209-2308

RHETT BUTLER
IRIS
1616 N. FORT MEYER DRIVE
SUITE 1050
ARLINGTON, VA 22209

CATHERINE DE GROOT-HEDLIN
SCRIPPS INSTITUTION OF OCEANOGRAPHY
UNIVERSITY OF CALIFORNIA, SAN DIEGO
INSTITUTE OF GEOPHYSICS AND PLANETARY PHYSICS
LA JOLLA, CA 92093

SEAN DORAN
ACIS
DCI/ACIS
WASHINGTON , DC 20505

RICHARD J. FANTEL
BUREAU OF MINES
DEPT OF INTERIOR, BLDG 20
DENVER FEDERAL CENTER
DENVER, CO 80225

RALPH ALEWINE
NTPO
1901 N. MOORE STREET, SUITE 609
ARLINGTON, VA 22209

MUAWIA BARAZANGI
INSTITUTE FOR THE STUDY OF THE CONTINENTS
3126 SNEE HALL
CORNELL UNIVERSITY
ITHACA, NY 14853

T.G. BARKER
MAXWELL TECHNOLOGIES
P.O. BOX 23558
SAN DIEGO, CA 92123

THERON J. BENNETT
MAXWELL TECHNOLOGIES
11800 SUNRISE VALLEY DRIVE SUITE 1212
RESTON, VA 22091

JONATHAN BERGER
UNIVERSITY OF CA, SAN DIEGO
SCRIPPS INSTITUTION OF OCEANOGRAPHY IGPP, 0225
9500 GILMAN DRIVE
LA JOLLA, CA 92093-0225

STEVEN BRATT
NTPO
1901 N. MOORE STREET, SUITE 609
ARLINGTON, VA 22209

LESLIE A. CASEY
DOE
1000 INDEPENDENCE AVE. SW
NN-40
WASHINGTON, DC 20585-0420

STANLEY DICKINSON
AFOSR
110 DUNCAN AVENUE, SUITE B115
BOLLING AFB
WASHINGTON, D.C. 20332-001

DIANE I. DOSER
DEPARTMENT OF GEOLOGICAL SCIENCES
THE UNIVERSITY OF TEXAS AT EL PASO
EL PASO, TX 79968

JOHN FILSON
ACIS/TMG/NTT
ROOM 6T11 NHB
WASHINGTON, DC 20505

MARK D. FISK
MISSION RESEARCH CORPORATION
735 STATE STREET
P.O. DRAWER 719
SANTA BARBARA, CA 93102-0719

LORI GRANT
MULTIMAX, INC.
311C FOREST AVE. SUITE 3
PACIFIC GROVE, CA 93950

I. N. GUPTA
MULTIMAX, INC.
1441 MCCORMICK DRIVE
LARGO, MD 20774

JAMES HAYES
NSF
4201 WILSON BLVD., ROOM 785
ARLINGTON, VA 22230

MICHAEL HEDLIN
UNIVERSITY OF CALIFORNIA, SAN DIEGO
SCRIPPS INSTITUTION OF OCEANOGRAPHY IGPP, 0225
9500 GILMAN DRIVE
LA JOLLA, CA 92093-0225

EUGENE HERRIN
SOUTHERN METHODIST UNIVERSITY
DEPARTMENT OF GEOLOGICAL SCIENCES
DALLAS, TX 75275-0395

VINDELL HSU
HQ/AFTAC/TTR
1030 S. HIGHWAY A1A
PATRICK AFB, FL 32925-3002

RONG-SONG JIH
PHILLIPS LABORATORY
EARTH SCIENCES DIVISION
29 RANDOLPH ROAD
HANSCOM AFB, MA 01731-3010

LAWRENCE LIVERMORE NATIONAL LABORATORY
ATTN: TECHNICAL STAFF (PLS ROUTE)
PO BOX 808, MS L-200
LIVERMORE, CA 94551

LAWRENCE LIVERMORE NATIONAL LABORATORY
ATTN: TECHNICAL STAFF (PLS ROUTE)
PO BOX 808, MS L-221
LIVERMORE, CA 94551

ROBERT GEIL
DOE
PALAIS DES NATIONS, RM D615
GENEVA 10, SWITZERLAND

HENRY GRAY
SMU STATISTICS DEPARTMENT
P.O. BOX 750302
DALLAS, TX 75275-0302

DAVID HARKRIDER
PHILLIPS LABORATORY
EARTH SCIENCES DIVISION
29 RANDOLPH ROAD
HANSCOM AFB, MA 01731-3010

THOMAS HEARN
NEW MEXICO STATE UNIVERSITY
DEPARTMENT OF PHYSICS
LAS CRUCES, NM 88003

DONALD HELMBERGER
CALIFORNIA INSTITUTE OF TECHNOLOGY
DIVISION OF GEOLOGICAL & PLANETARY SCIENCES
SEISMOLOGICAL LABORATORY
PASADENA, CA 91125

ROBERT HERRMANN
ST. LOUIS UNIVERSITY
DEPARTMENT OF EARTH & ATMOSPHERIC SCIENCES
3507 LACLEDE AVENUE
ST. LOUIS, MO 63103

ANTHONY IANNACCHIONE
BUREAU OF MINES
COCHRANE MILL ROAD
PO BOX 18070
PITTSBURGH, PA 15236-9986

THOMAS JORDAN
MASSACHUSETTS INSTITUTE OF TECHNOLOGY
EARTH, ATMOSPHERIC & PLANETARY SCIENCES
77 MASSACHUSETTS AVENUE, 54-918
CAMBRIDGE, MA 02139

LAWRENCE LIVERMORE NATIONAL LABORATORY
ATTN: TECHNICAL STAFF (PLS ROUTE)
PO BOX 808, MS L-207
LIVERMORE, CA 94551

LAWRENCE LIVERMORE NATIONAL LABORATORY
ATTN: TECHNICAL STAFF (PLS ROUTE)
LLNL
PO BOX 808, MS L-175
LIVERMORE, CA 94551

LAWRENCE LIVERMORE NATIONAL LABORATORY
ATTN: TECHNICAL STAFF (PLS ROUTE)
PO BOX 808, MS L-208
LIVERMORE, CA 94551

LAWRENCE LIVERMORE NATIONAL LABORATORY
ATTN: TECHNICAL STAFF (PLS ROUTE)
PO BOX 808, MS L-195
LIVERMORE, CA 94551

THORNE LAY
UNIVERSITY OF CALIFORNIA, SANTA CRUZ
EARTH SCIENCES DEPARTMENT
EARTH & MARINE SCIENCE BUILDING
SANTA CRUZ, CA 95064

DONALD A. LINGER
DNA
6801 TELEGRAPH ROAD
ALEXANDRIA, VA 22310

LOS ALAMOS NATIONAL LABORATORY
ATTN: TECHNICAL STAFF (PLS ROUTE)
PO BOX 1663, MS F665
LOS ALAMOS, NM 87545

LOS ALAMOS NATIONAL LABORATORY
ATTN: TECHNICAL STAFF (PLS ROUTE)
PO BOX 1663, MS C335
LOS ALAMOS, NM 87545

KEITH MCLAUGHLIN
MAXWELL TECHNOLOGIES
P.O. BOX 23558
SAN DIEGO, CA 92123

RICHARD MORROW
USACDA/IVI
320 21ST STREET, N.W.
WASHINGTON, DC 20451

JAMES NI
NEW MEXICO STATE UNIVERSITY
DEPARTMENT OF PHYSICS
LAS CRUCES, NM 88003

PACIFIC NORTHWEST NATIONAL LABORATORY
ATTN: TECHNICAL STAFF (PLS ROUTE)
PO BOX 999, MS K6-48
RICHLAND, WA 99352

LAWRENCE LIVERMORE NATIONAL LABORATORY
ATTN: TECHNICAL STAFF (PLS ROUTE)
PO BOX 808, MS L-202
LIVERMORE, CA 94551

LAWRENCE LIVERMORE NATIONAL LABORATORY
ATTN: TECHNICAL STAFF (PLS ROUTE)
PO BOX 808, MS L-205
LIVERMORE, CA 94551

ANATOLI L. LEVSHIN
DEPARTMENT OF PHYSICS
UNIVERSITY OF COLORADO
CAMPUS BOX 390
BOULDER, CO 80309-0309

LOS ALAMOS NATIONAL LABORATORY
ATTN: TECHNICAL STAFF (PLS ROUTE)
PO BOX 1663, MS F659
LOS ALAMOS, NM 87545

LOS ALAMOS NATIONAL LABORATORY
ATTN: TECHNICAL STAFF (PLS ROUTE)
PO BOX 1663, MS D460
LOS ALAMOS, NM 87545

GARY MCCARTOR
SOUTHERN METHODIST UNIVERSITY
DEPARTMENT OF PHYSICS
DALLAS, TX 75275-0395

BRIAN MITCHELL
DEPARTMENT OF EARTH & ATMOSPHERIC SCIENCES
ST. LOUIS UNIVERSITY
3507 LACLEDE AVENUE
ST. LOUIS, MO 63103

JOHN MURPHY
MAXWELL TECHNOLOGIES
11800 SUNRISE VALLEY DRIVE SUITE 1212
RESTON, VA 22091

JOHN ORCUTT
INSTITUTE OF GEOPHYSICS AND PLANETARY PHYSICS
UNIVERSITY OF CALIFORNIA, SAN DIEGO
LA JOLLA, CA 92093

PACIFIC NORTHWEST NATIONAL LABORATORY
ATTN: TECHNICAL STAFF (PLS ROUTE)
PO BOX 999, MS K7-34
RICHLAND, WA 99352

PACIFIC NORTHWEST NATIONAL LABORATORY
ATTN: TECHNICAL STAFF (PLS ROUTE)
PO BOX 999, MS K6-40
RICHLAND, WA 99352

PACIFIC NORTHWEST NATIONAL LABORATORY
ATTN: TECHNICAL STAFF (PLS ROUTE)
PO BOX 999, MS K5-72
RICHLAND, WA 99352

PACIFIC NORTHWEST NATIONAL LABORATORY
ATTN: TECHNICAL STAFF (PLS ROUTE)
PO BOX 999, MS K5-12
RICHLAND, WA 99352

KEITH PRIESTLEY
DEPARTMENT OF EARTH SCIENCES
UNIVERSITY OF CAMBRIDGE
MADINGLEY RISE, MADINGLEY ROAD
CAMBRIDGE, CB3 OEZ UK

PAUL RICHARDS
COLUMBIA UNIVERSITY
LAMONT-DOHERTY EARTH OBSERVATORY
PALISADES, NY 10964

CHANDAN SAIKIA
WOOODWARD-CLYDE FEDERAL SERVICES
566 EL DORADO ST., SUITE 100
PASADENA, CA 91101-2560

SANDIA NATIONAL LABORATORY
ATTN: TECHNICAL STAFF (PLS ROUTE)
DEPT. 6116
MS 0750, PO BOX 5800
ALBUQUERQUE, NM 87185-0750

SANDIA NATIONAL LABORATORY
ATTN: TECHNICAL STAFF (PLS ROUTE)
DEPT. 9311
MS 1159, PO BOX 5800
ALBUQUERQUE, NM 87185-1159

SANDIA NATIONAL LABORATORY
ATTN: TECHNICAL STAFF (PLS ROUTE)
DEPT. 5736
MS 0655, PO BOX 5800
ALBUQUERQUE, NM 87185-0655

THOMAS SERENO JR.
SCIENCE APPLICATIONS INTERNATIONAL
CORPORATION
10260 CAMPUS POINT DRIVE
SAN DIEGO, CA 92121

PACIFIC NORTHWEST NATIONAL LABORATORY
ATTN: TECHNICAL STAFF (PLS ROUTE)
PO BOX 999, MS K7-22
RICHLAND, WA 99352

PACIFIC NORTHWEST NATIONAL LABORATORY
ATTN: TECHNICAL STAFF (PLS ROUTE)
PO BOX 999, MS K6-84
RICHLAND, WA 99352

FRANK PILOTTE
HQ/AFTAC/TT
1030 S. HIGHWAY A1A
PATRICK AFB, FL 32925-3002

JAY PULLI
RADIX SYSTEMS, INC.
6 TAFT COURT
ROCKVILLE, MD 20850

DAVID RUSSELL
HQ AFTAC/TTR
1030 SOUTH HIGHWAY A1A
PATRICK AFB, FL 32925-3002

SANDIA NATIONAL LABORATORY
ATTN: TECHNICAL STAFF (PLS ROUTE)
DEPT. 5704
MS 0979, PO BOX 5800
ALBUQUERQUE, NM 87185-0979

SANDIA NATIONAL LABORATORY
ATTN: TECHNICAL STAFF (PLS ROUTE)
DEPT. 5791
MS 0567, PO BOX 5800
ALBUQUERQUE, NM 87185-0567

SANDIA NATIONAL LABORATORY
ATTN: TECHNICAL STAFF (PLS ROUTE)
DEPT. 5704
MS 0655, PO BOX 5800
ALBUQUERQUE, NM 87185-0655

SANDIA NATIONAL LABORATORY
ATTN: TECHNICAL STAFF (PLS ROUTE)
DEPT. 6116
MS 0750, PO BOX 5800
ALBUQUERQUE, NM 87185-0750

AVI SHAPIRA
SEISMOLOGY DIVISION
THE INSTITUTE FOR PETROLEUM RESEARCH AND
GEOPHYSICS
P.O.B. 2286, NOLON 58122 ISRAEL

ROBERT SHUMWAY
410 MRAK HALL
DIVISION OF STATISTICS
UNIVERSITY OF CALIFORNIA
DAVIS, CA 95616-8671

DAVID SIMPSON
IRIS
1616 N. FORT MEYER DRIVE
SUITE 1050
ARLINGTON, VA 22209

BRIAN SULLIVAN
BOSTON COLLEGE
INSITUTE FOR SPACE RESEARCH
140 COMMONWEALTH AVENUE
CHESTNUT HILL, MA 02167

NAFI TOKSOZ
EARTH RESOURCES LABORATORY, M.I.T.
42 CARLTON STREET, E34-440
CAMBRIDGE, MA 02142

GREG VAN DER VINK
IRIS
1616 N. FORT MEYER DRIVE
SUITE 1050
ARLINGTON, VA 22209

TERRY WALLACE
UNIVERSITY OF ARIZONA
DEPARTMENT OF GEOSCIENCES
BUILDING #77
TUCSON, AZ 85721

JAMES WHITCOMB
NSF
NSF/ISC OPERATIONS/EAR-785
4201 WILSON BLVD., ROOM785
ARLINGTON, VA 22230

JIAKANG XIE
COLUMBIA UNIVERSITY
LAMONT DOHERTY EARTH OBSERVATORY
ROUTE 9W
PALISADES, NY 10964

OFFICE OF THE SECRETARY OF DEFENSE
DDR&E
WASHINGTON, DC 20330

TACTEC
BATTELLE MEMORIAL INSTITUTE
505 KING AVENUE
COLUMBUS, OH 43201 (FINAL REPORT)

MATTHEW SIBOL
ENSCO, INC.
445 PINEDA COURT
MELBOURNE, FL 32940

JEFFRY STEVENS
MAXWELL TECHNOLOGIES
P.O. BOX 23558
SAN DIEGO, CA 92123

DAVID THOMAS
ISEE
29100 AURORA ROAD
CLEVELAND, OH 44139

LAWRENCE TURNBULL
ACIS
DCI/ACIS
WASHINGTON, DC 20505

FRANK VERNON
UNIVERSITY OF CALIFORNIA, SAN DIEGO
SCRIPPS INSTITUTION OF OCEANOGRAPHY IGPP, 0225
9500 GILMAN DRIVE
LA JOLLA, CA 92093-0225

DANIEL WEILL
NSF
EAR-785
4201 WILSON BLVD., ROOM 785
ARLINGTON, VA 22230

RU SHAN WU
UNIVERSITY OF CALIFORNIA SANTA CRUZ
EARTH SCIENCES DEPT.
1156 HIGH STREET
SANTA CRUZ, CA 95064

JAMES E. ZOLLWEG
BOISE STATE UNIVERSITY
GEOSCIENCES DEPT.
1910 UNIVERSITY DRIVE
BOISE, ID 83725

DEFENSE TECHNICAL INFORMATION CENTER
8725 JOHN J. KINGMAN ROAD
FT BELVOIR, VA 22060-6218 (2 COPIES)

PHILLIPS LABORATORY
ATTN: XPG
29 RANDOLPH ROAD
HANSCOM AFB, MA 01731-3010

PHILLIPS LABORATORY
ATTN: GPE
29 RANDOLPH ROAD
HANSCOM AFB, MA 01731-3010

PHILLIPS LABORATORY
ATTN: TSML
5 WRIGHT STREET
HANSCOM AFB, MA 01731-3004

PHILLIPS LABORATORY
ATTN: PL/SUL
3550 ABERDEEN AVE SE
KIRTLAND, NM 87117-5776 (2 COPIES)